Breakaway Pole Coupling
for New or Retrofitted Poles
Patent # 7,056,056
Report PSA-3

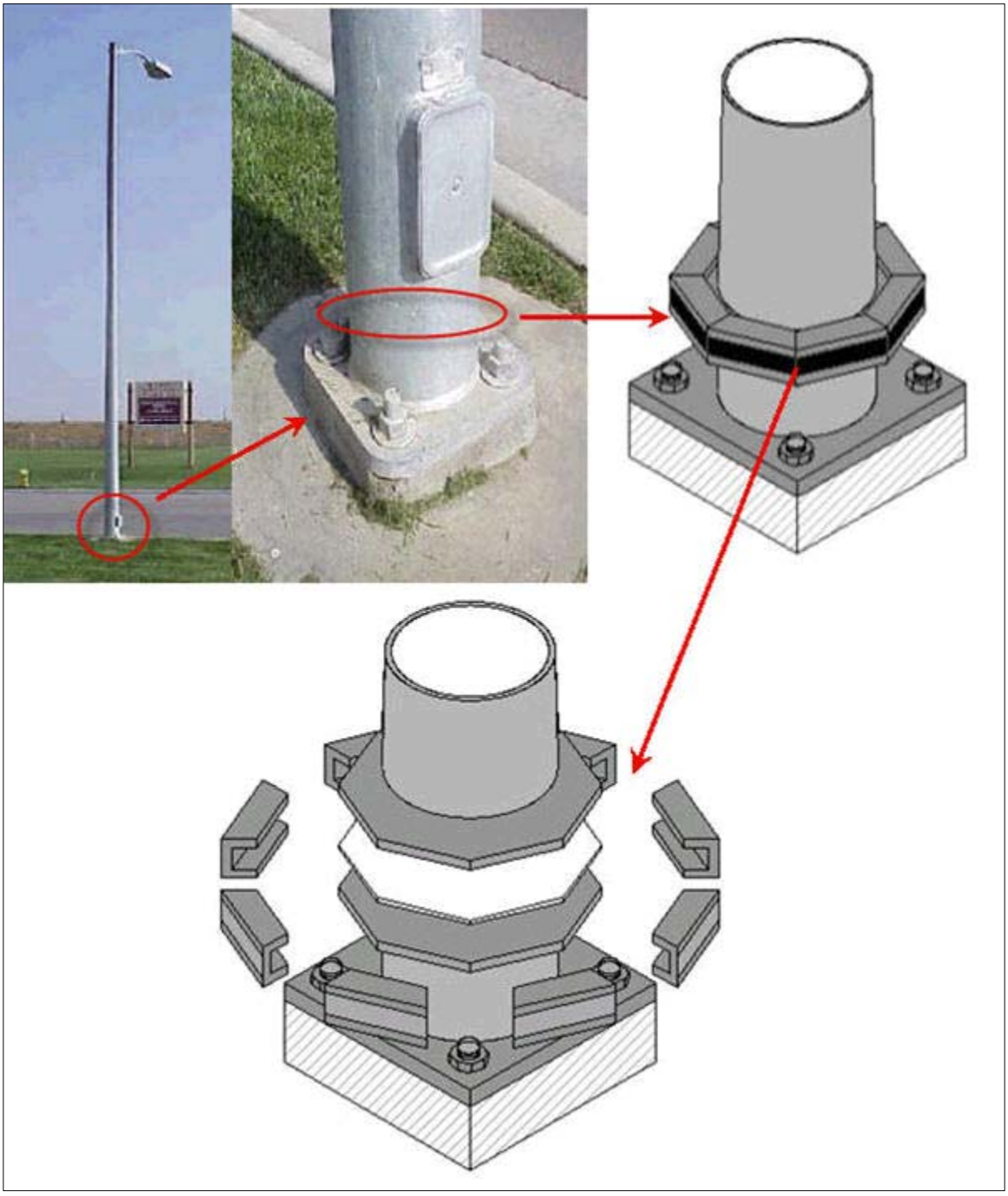

PolyTechnic SoftWare Associates
Stuart Larsen & Ken Wiegand
805-654-1344 & 530-518-4059

Table of Contents

2.0 Introduction and Concept Description

Introduction

A new **breakaway device** used to convert existing or create new highway obstacles into improved crashworthy obstacles is presented.

The device is referred to in this presentation as a **Shear Coupling**.

This **Shear Coupling** may be used to retrofit exiting or incorporated into new light poles, telephone poles, or sign/signal poles.

The **Shear Coupling** will be shown to accomodate all necessary static service loads; and further, will be shown to fail dynamically in such a manner as to meet all crashworthy requirements of the **1985 AASHTO** specifications.

An important advantage of this new **Shear Coupling** is that the failure mode is such that a de-masted pole may be reset on site without the need for any major structural components from the manufacturer. Damaged accessories attached to the pole may need replacement, but the pole, supporting base, and **Shear Coupler** may be reset immediately.

Concept Description

A **generic** light pole is selected as a standard for the comparative analysis approach discussed in Section 1.0.

A typical highway light pole is selected as a **standard design** which is to be modified or retrofitted with a new breakaway shear coupling. The selected standard light pole, shown in Figure 2.0.1, is located along California Highway 5 in the city of Santa Nella.

This generic light pole is approximately **35 - 40** feet high supporting a **6 to 8** foot span light. The diameter of the base of the pole is approximately **8** inches and appeares to taper to approximately 4 inches at the top. Although the pole wall thickness at the base could not be conveniently measured it is estimated to be **3/8** inch.

The total weigth of the pole is estimated at **265 lb**.

Figure 2.0.1

The supporting pole base plate is **1 inch** thick, **12 inches** square, with 4 **1 inch diameter bolts** on an approximately **10.5 inch** diameter circle (See Figure 2.0.2).

These estimated dimensions are not exact, but will be used as a standard for the comparative analysis approach.

These dimensions, however, have been checked and compared to a similiar class of highway ligh poles manufactured by **Millerberend Manufacturing Company** in Winsted, Minnesota. Data, obtained from their web-site, is attached within the appendix, and suggests that the above selected geometry is reasonable.

Figure 2.0.2

The identification plate attached to the pole is shown in Figure 2.0.3.

The identification plate identifies the pole as a **TYPE 15-95** pole, followed by what may be a serial or location number.

The manufacturer of the specific light pole shown in Figures 2.0.1 through 2.0.3 is unknown at the time of this writing.

Figure 2.0.3

The light pole shown in Figure 2.0.2 is retrofitted with a breakaway shear coupling as shown in Figure 2.0.4.

The pole is cut between the base and the wiring acess cover shown in Figure 2.0.2 and the bottom plate of the shear coupling welded to the pole.

The remaining top portion of the light pole is welded to the top plate of the shear coupling and then reassembled as shown in Figure 2.0.4. The wiring access panel is omitted.

The shear coupling has an octagon shape, the outer diameter being the same **12"** dimension of the generic pole support base. The thickness of the coupling is approximately **2"**, or twice the thickness of the base.

These general dimensions would be scaled up to accomodate a larger light pole, signal, or road sign structure which is supported by a four bolt pattern base.

The octagon plates welded to the bottom and top cut sections of the light pole are held together with **8 edge caps**. The **8 edge caps** are held in place by a steel strap, symmetrically placed around the outer circumference of the edge caps, and tightened to a specified stress level.

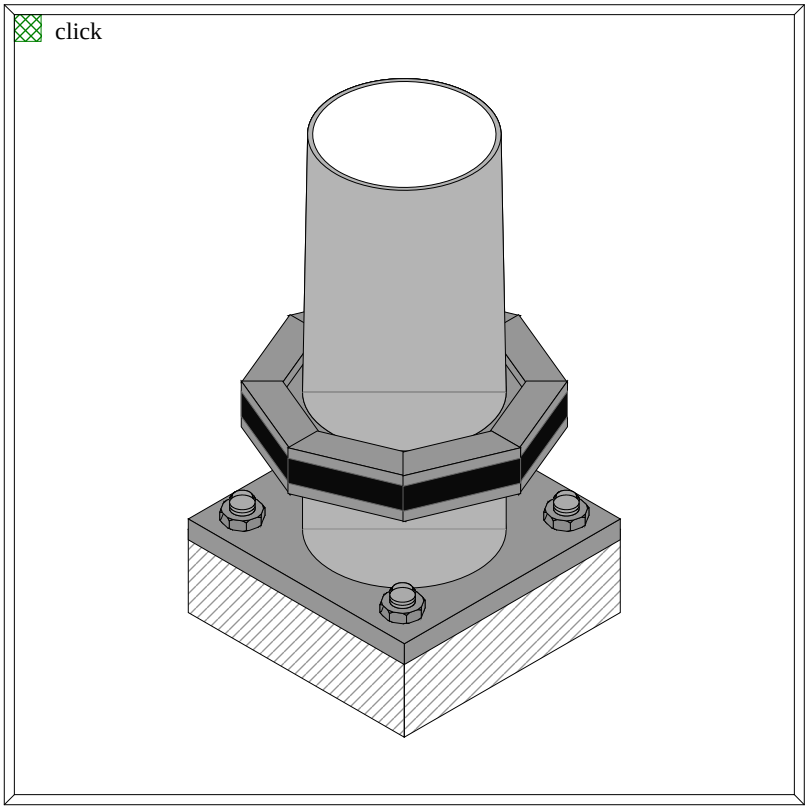

Figure 2.0.4

Figure 2.0.5 shows the steel strap removed and the **8 edge caps** radially exploded exposing the top and bottom octagon plates welded to the top and bottom sections of the light pole.

Details of the octagon plate and a typical edge cap are shown in Figures 2.0.6 and 2.0.7.

D_p = Diameter of the octagon plate.

L_{pe} = Length of octagon plate edge.

t_p = Thickness of octagon plate.

W_t = Web thickness.

W_h = Web height.

F_t = Flange thickness.

F_{wo} = Flange outer width.

F_{wi} = Flange inner width.

F_{wm} = Flange mean width.

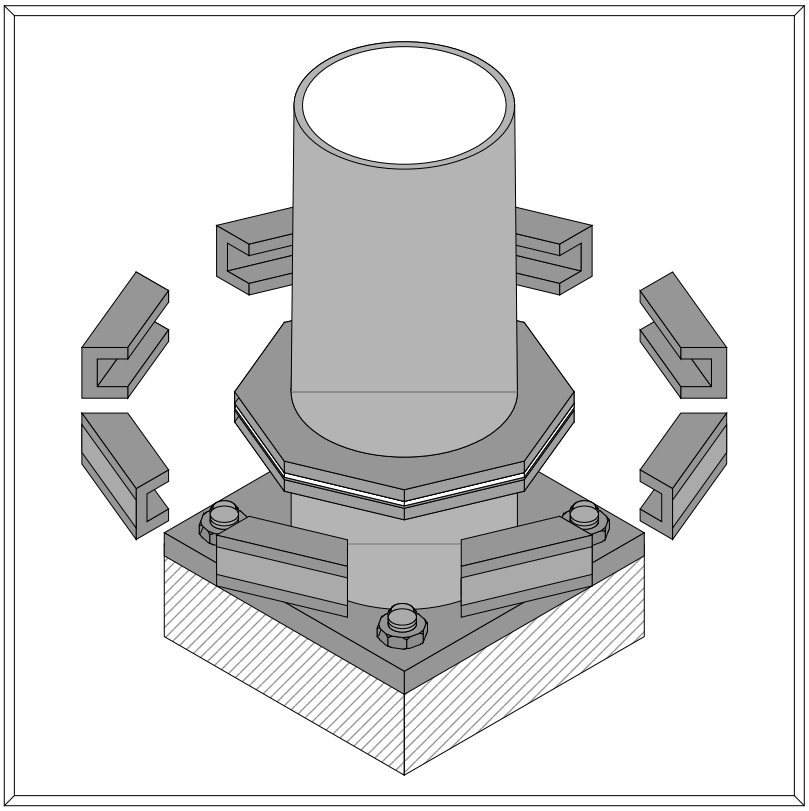

Figure 2.0.5

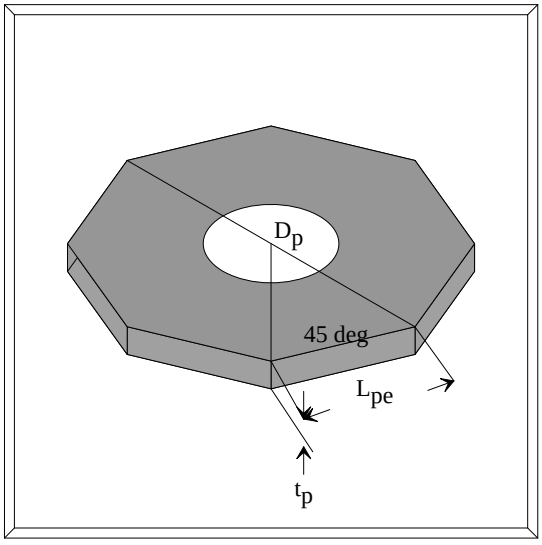

Figure 2.0.6

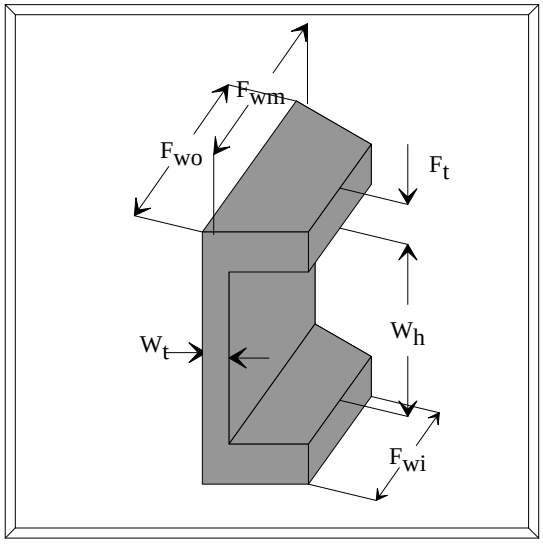

Figure 2.0.7

For the standard generic pole being used within this report, these parameters become...

D_p = **6"** L_{pe} = **4.592"** t_p = **1"**

W_t = **0.5"** W_h = **2.2"**

F_t = **0.5"** F_{wo} = **5.006"** F_{wi} = **4.118"** F_{wm} = **4.799"**

Next, the pole is exploded vertically exposing the full details of the shear coupling assembly.

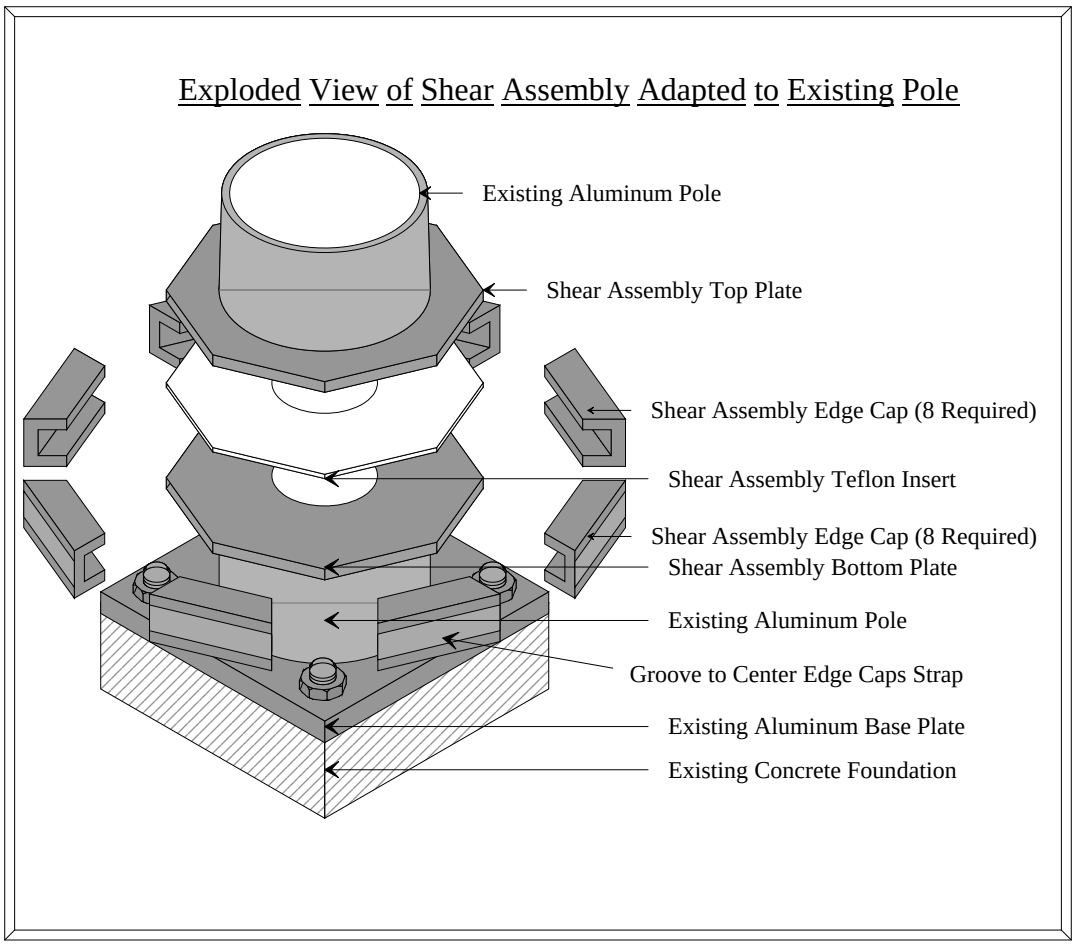

Figure 2.0.8

A teflon insert is placed between the top and bottom plates of the shear coupling to prevent galling of the surfaces over time and to enhance or control the horizontal force required to shear or fail the coupling. A **0.2"** thick teflon insert has been used in this example.

The above specific dimensions are being used as **proof of concept** of the shear coupling's ability to support all the **static service** normal, axial, bending, and torsional loads. Slight changes may provide a more cost effective design. The use, for example, of available extruded sections for the edge caps, may drive the final dimensions. This additional engineering design is unnecessary until **proof of concept** is established.

The **static analysis** is presented in **Section 3**.

As a vehicle impacts the pole, the dynamic forces, which of course exceed the static service loads, cause the shear coupling top plate to slide horizonally relative to the bottom plate. The steel strap binding the edge caps in place elongates and finally breaks. The edge caps are released permitting the pole to separate horizontally in a controlled manner.

The **dynamic analysis** is presented in **Section 4**.

3.0 Analysis Approach

The foundation, base plate and bolt pattern of the generic light pole discussed in **Section 2.0** is repeated in Figure 3.0.1.

It is assumed that the base plate and pole attachment meets all necessary static service load requirements.

The maximum allowable bending moment, axial load, shear load, and torsional load for this generic base and pole attachment are computed **in terms of** the allowable normal σ_{all} and allowable shear τ_{all} stresses of the bolt material.

It is further assumed that the pole, slightly above the base weldment also meets all necessary static service load requirements.

The maximum allowable bending moment, axial load, shear load, and torsional load for this generic pole are computed **in terms of** the allowable normal σ_{all} and allowable shear τ_{all} stresses of the pole material.

Figure 3.0.1

A web search of highway pole manufacturers, (see attached data in the Appendix), suggests the use of a high strength aluminum alloy for such light poles which exhibit yield stresses of the 50,000 psi level. These yield stresses are, of course, lowered by safety factors and code requirements to **allowable stress levels**. It is assumed that these allowable normal σ_{all} and allowable shear stresses τ_{all} are approximately the same as the attachment bolts and the high strength aluminum alloy pole material.

Finally, the maximum allowable bending moment, axial load, shear load, and torsional load for the installed **Shear Coupling** are computed **in terms of** the allowable normal σ_{all} and allowable shear τ_{all} stresses of the **Shear Coupling** material. It is assumed that the **Shear Coupling** material is the same high strength aluminum used for the pole.

The maximum allowable bending moment, axial load, shear load, and torsional load for the **Shear Coupling** in terms of the allowable normal σ_{all} and allowable shear τ_{all} stresses are then compared to those of the base attachment and pole. If they meet or exceed those of the base attachment and pole then the **Shear Coupling** qualifies as meeting all necessary code requirements.

For this generic pole, the **Shear Coupling** geometry is set with reference to the dimensions of the pole attachment base.

As a consequence, this type of **comparative analysis** qualifies **Shear Couplings** for all sizes of highway pole obstacles as long as the relative geometry of the **Shear Coupling** to base attachment is reained.

3.1 Analysis of the Pole Base

3.1.1 Pole Base: Allowable Bending Moment

The applied bending moment to the pole located near the base is shown in Figure 3.1.1.1.

A short segment of the attached vertical pole is shown to emphasize the additional stiffness provided to the base plate due to the presence of the welded pole.

The base plate is assumed to rotate about an axis passing through the two opposite bolts as shown in Figure 3.1.1.1.

Assuming the stiffness of the base plate and welded pole assembly is large compared to the axial stiffness of bolts, the allowable bending moment $\mathbf{M_{all}}$ will be reached when the normal stress in the bolts have reached their allowable normal stress.

The geometry of the base plate and bolt locations are shown in Figure 3.1.1.1.

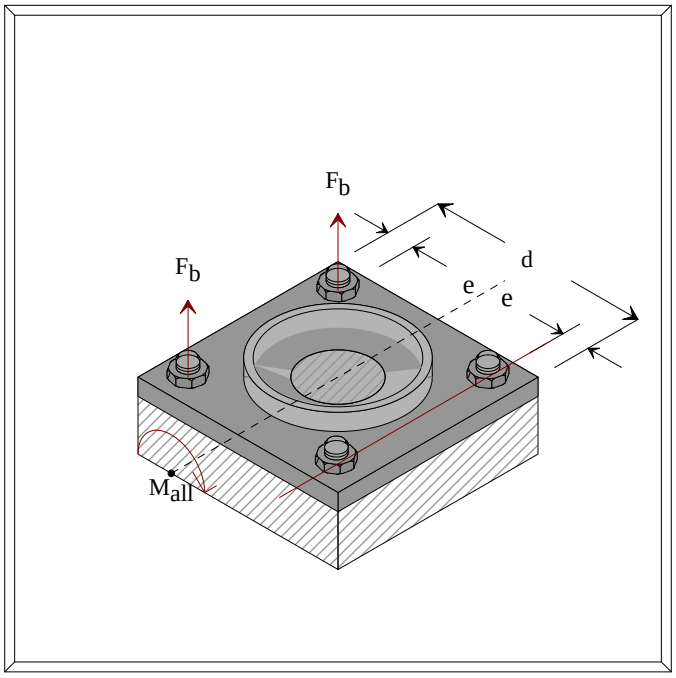

Figure 3.1.1.1

The allowable bending moment would be...

$$M_{all} = 2 * (d - e) * A_b * \sigma_{all}$$

where the area of a bolt $\mathbf{A_b}$ is...

$$A_b = \frac{\pi}{4} * d_b^{\,2}$$

where $\mathbf{d_b}$ is the bolt diameter.

$$M_{all} = 2 * (d - e) * \frac{\pi}{4} * d_b^{\,2} * \sigma_{all}$$

$$M_{all} = (d - e) * \frac{\pi}{2} * d_b^{\,2} * \sigma_{all} \quad \text{---------- Eq. 3.1.1.1}$$

Letting...
d = 12 in.
e = 1.5 in.
$\mathbf{d_b}$ **= 1.0** in.

The allowable moment from Equation 3.1.1.1 would be...

$$M_{all} = 16.49 * \sigma_{all} \qquad \text{Eq. 3.1.1.2}$$

Equation 3.1.1.2 states that given an allowable normal stress, the pole could support **16.49 in-lbs** of moment for each available psi of bolt material strength.

3.1 Analysis of the Pole Base

3.1.2 Pole Base: Allowable Normal Force

The applied normal force to the pole located near the center of the base is shown in Figure 3.1.2.1.

A short segment of the attached vertical pole is shown to emphasize the additional stiffness provided to the base plate due to the presence of the welded pole.

The applied normal force is equilibrated by equal normal forces in each of the four bolts.

The geometry of the base plate and bolt locations are shown in Figure 3.1.2.1.

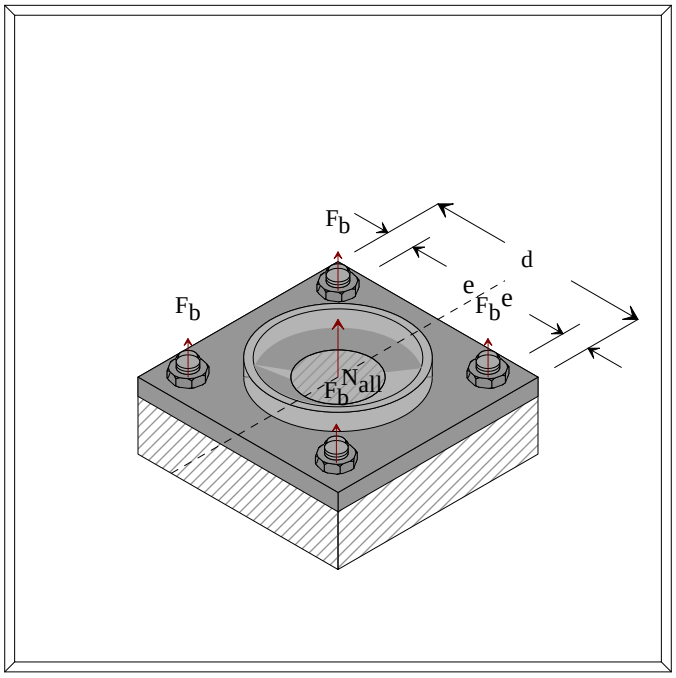

Figure 3.1.2.1

The allowable normal force would be...

$$N_{all} = 4 * A_b * \sigma_{all}$$

where the area of a bolt $\mathbf{A_b}$ is...

$$A_b = \frac{\pi}{4} * d_b^{\,2}$$

where $\mathbf{d_b}$ is the bolt diameter.

$$N_{all} = 4 * \left(\frac{1}{4} * \pi * d_b^{\,2} \right) * \sigma_{all}$$

$$N_{all} = \pi * d_b^{\,2} * \sigma_{all} \quad \text{---------- Eq. 3.1.2.1}$$

Letting...
d = 12 in.
e = 1.5 in.
$\mathbf{d_b}$ **= 1.0** in.

The allowable normal force from Equation 3.1.2.1 would be...

$$N_{all} = 3.14 * \sigma_{all} \quad \text{---------- Eq. 3.1.2.2}$$

Equation 3.1.2.2 states that given an allowable normal stress, the pole could support **3.14 lbs** of upward axial load for each available psi of bolt material strength.

3.1 Analysis of the Pole Base

3.1.3 Pole Base: Allowable Torsion

The applied normal force to the pole located near the center of the base is shown in Figure 3.1.3.1.

A short segment of the attached vertical pole is shown to emphasize the additional stiffness provided to the base plate due to the presence of the welded pole.

The applied torque is equilibrated by equal shear forces in each of the four bolts.

The geometry of the base plate and bolt locations are shown in Figure 3.1.3.1.

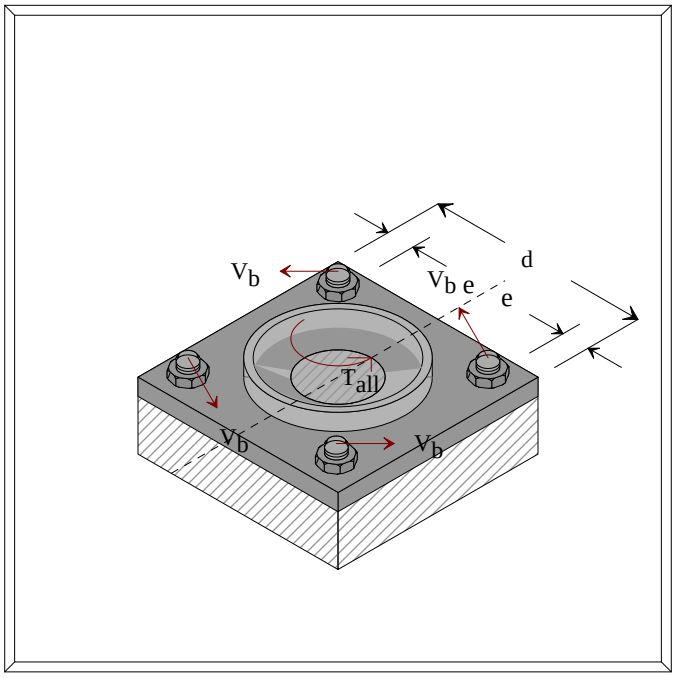

Figure 3.1.3.1

The allowable moment would be...

$$T_{all} = 4 * r_b * A_b * \tau_{all}$$

where d_b is the perpendicular distance from the center to the line of action of each bolt shear force, and would be...

$$r_b = \sqrt{\left(\frac{d_p}{2} - e\right)^2 + \left(\frac{d_p}{2} - e\right)^2}$$

$$r_b = \sqrt{\left(\frac{12.0}{2} - 1.5\right)^2 + \left(\frac{12.0}{2} - 1.5\right)^2} \quad \text{Eq. 3.1.3.0C} \quad \text{Eq. 3.1.3.0O}$$

where the area of a bolt $\mathbf{A_b}$ in terms of the diameter of the bolt d_b is...

$$A_b = \frac{\pi}{4} * d_b^2$$

$$T_{all} = 4 * r_b * \left(\frac{1}{4} * \pi * d_b^2\right) * \tau_{all}$$

$$T_{all} = \pi * r_b * d_b^2 * \tau_{all} \quad \text{Eq. 3.1.3.1}$$

Letting...
d = 12 in.
e = 1.5 in.
d_b = 1.0 in.
r_b = 6.36

The allowable moment from Equation 3.1.3.1 would be...

$$T_{all} = 19.98 * \tau_{all}$$ Eq. 3.1.3.2

Equation 3.1.3.2 states that given an allowable shear stress, the pole could support **19.98 in-lbs** of torsional load for each available psi of bolt material strength.

3.1 Analysis of the Pole Base

3.1.4 Pole Base: Allowable Shear Force

The applied shear force to the pole located near the center of the base is shown in Figure 3.1.4.1.

A short segment of the attached vertical pole is shown to emphasize the additional stiffness provided to the base plate due to the presence of the welded pole.

The applied shear is equilibrated by equal shear forces in each of the four bolts.

The geometry of the base plate and bolt locations are shown in Figure 3.1.4.1.

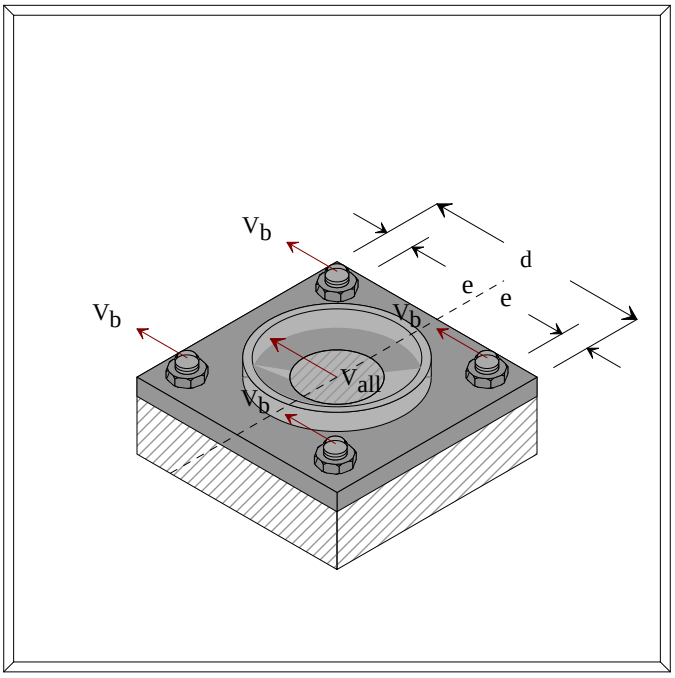

Figure 3.1.4.1

The allowable shear would be...

$$V_{all} = 4 * A_b * \tau_{all}$$

where the area of a bolt $\mathbf{A_b}$ in terms of the diameter of the bolt d_b is...

$$A_b = \frac{\pi}{4} * d_b^{\,2}$$

$$V_{all} = 4 * \left(\frac{1}{4} * \pi * d_b^{\,2} \right) * \tau_{all}$$

Vall=p*db^2*tall Letting... $\mathbf{d_b = 1.0}$ in.

The allowable shear from Equation 3.1.4.1 would be...

$$vall = 3.1416 * \tau_{all} \qquad \text{Eq. 3.1.4.1}$$

Equation 3.1.4.2 states that given an allowable shear stress, the pole could support **3.1416 lbs** of shear load for each available psi of bolt material strength.

3.2 Analysis of Pole

3.2.1 Pole: Allowable Bending Moment

The applied bending moment to the pole located near the base is shown in Figure 3.2.1.1

The allowable normal stress due to bending is provided by the conventional flexure equation...

$$\sigma_{all} = \frac{(M_{all} * y)}{I_p}$$

$$M_{all} = \frac{I_p}{c} * \sigma_{all}$$

The moment of inertia would be...

$$I_p = \frac{\pi}{64} * \left(d_o^{\,4} - d_i^{\,4}\right)$$

where $\mathbf{d_o}$ and $\mathbf{d_i}$ are the outer and inner diameters of the pole.

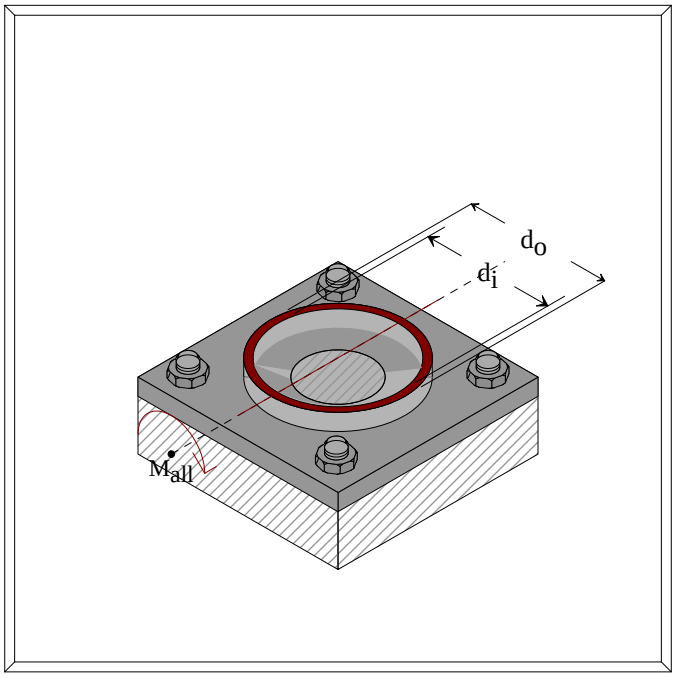

Figure 3.2.1.1

$$M_{all} = \frac{(\pi * \sigma_{all})}{(64 * c)} * \left(d_o^{\,4} - d_i^{\,4}\right) \quad \text{---------- Eq. 3.2.1.1}$$

Letting...
$\mathbf{d_o}$ **= 8** in.
$\mathbf{d_i}$ **= 7.25** in

This represents a wall thickness of **3/8 in**.

The allowable moment from Equation 3.2.1.1 would be...

$$M_{all} = 16.35 * \sigma_{all} \quad \text{---------- Eq. 3.2.1.2}$$

Equation 3.2.1.2 states that given an allowable normal stress, the pole could support **16.35 in-lbs** of moment for each available psi of material strength.

3.2.2 Analysis of Pole

3.2.2 Pole: Allowable Normal Force

The applied normal force to the pole located at the center of the base is shown in Figure 3.2.2.1

The applied normal force is equilibrated by a uniform distribution of normal stress aroud the circumference of the meam radius of the pole cross section. This distribution is simplified and shown by only two forces in Figure 3.2.2.1.

$$\sigma_{all} = \frac{N_{all}}{A_p}$$

$$N_{all} = A_p * \sigma_{all}$$

The cross section area of the pole near the base would be...

$$A_p = \frac{\pi}{4} * \left(d_o^{\,2} - d_i^{\,2} \right)$$

where $\mathbf{d_o}$ and $\mathbf{d_i}$ are the outer and inner diameters of the pole.

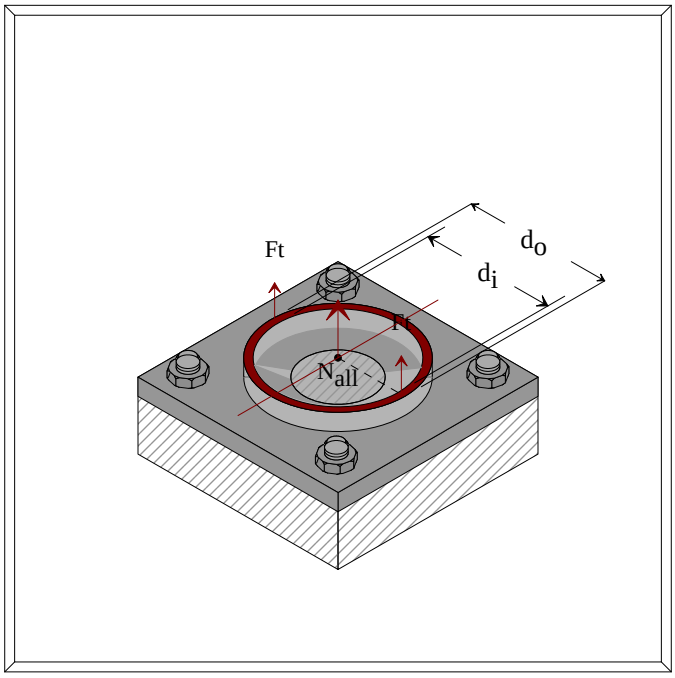

Figure 3.2.2.1

$$N_{all} = \frac{1}{4} * \pi * \sigma_{all} * \left(d_o^{\,4} - d_i^{\,4} \right) \quad \text{Eq. 3.2.2.1}$$

Letting...
$\mathbf{d_o}$ **= 8** in.
$\mathbf{d_i}$ **= 7.25** in

This represents a wall thickness of **3/8 in**.

The allowable moment from Equation 3.2.2.1 would be...

$$M_{all} = 8.98 * \sigma_{all} \quad \text{Eq. 3.2.2.2}$$

Equation 3.2.2.2 states that given an allowable normal stress, the pole could support **8.98 lbs** of upward axial load for each available psi of material strength.

3.2 Analysis of Pole

3.2.3 Pole: Allowable Torsion

The applied torque to the pole located at the center of the pole is shown in Figure 3.2.3.1

The applied torque is equilibrated by a uniform distribution of torsional shear stress around the circumference of the pole radius.

$$\tau_{all} = \frac{\left(T_{all} * \frac{d_o}{2}\right)}{Jp}$$

Tall=(2*Jp*tall)/do The polar moment of inertia J_p of the pole near the base would be...

$$Jp = \frac{\pi}{32} * \left(d_o^{\,4} - d_i^{\,4}\right)$$

where **d_o** and **d_i** are the outer and inner diameters of the pole.

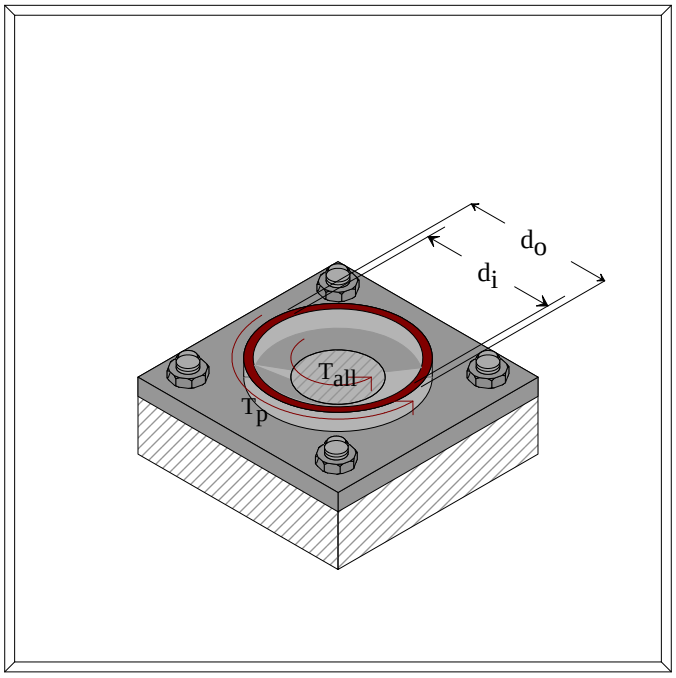

Figure 3.2.3.1

$$T_{all} = \frac{\left(\frac{\pi}{16} * \left(d_o^{\,4} - d_i^{\,4}\right) * \tau_{all}\right)}{d_o} \quad \text{---------- Eq. 3.2.3.1}$$

Letting...
d_o = 8 in.

d_i = 7.25 in

The allowable moment from Equation 3.2.3.1 would be...

$$T_{all} = 32.72 * \sigma_{all} \quad \text{---------- Eq. 3.2.3.2}$$

Equation 3.2.3.2 states that given an allowable normal stress, the pole could support **32.72 lbs** of upward axial load for each available psi of material strength.

3.2 Analysis of Pole

3.2.4 Pole: Allowable Shear Force

The applied horizontal shear to the pole is assumed at the center and is shown in Figure 3.2.4.1.

The applied shear is equilibtrated by a parabolic distribution of horizontal shear stress in the pole wall reaching a maximum at the centroid of the pole section. The maximum horizontal shear stress is provided by

$$\tau_{all} = \frac{(V_{all} * Q_{max})}{(I_p * (d_o - d_i))}$$

Q_{max} is the first moment of area of the pole cross section about the centroidal axis. Q_{max} and I_p may be shown to be...

$$Q_{max} = \left(\frac{1}{12}\right) * (d_o^{\,3} - Di^{\,3})$$

$$I_p = \frac{\pi}{64} * (d_o^{\,4} - d_i^{\,4}) \qquad \text{----------Eq. 3.2.4.1}$$

where $\mathbf{d_o}$ and $\mathbf{d_i}$ are the outer and inner diameters of the pole.

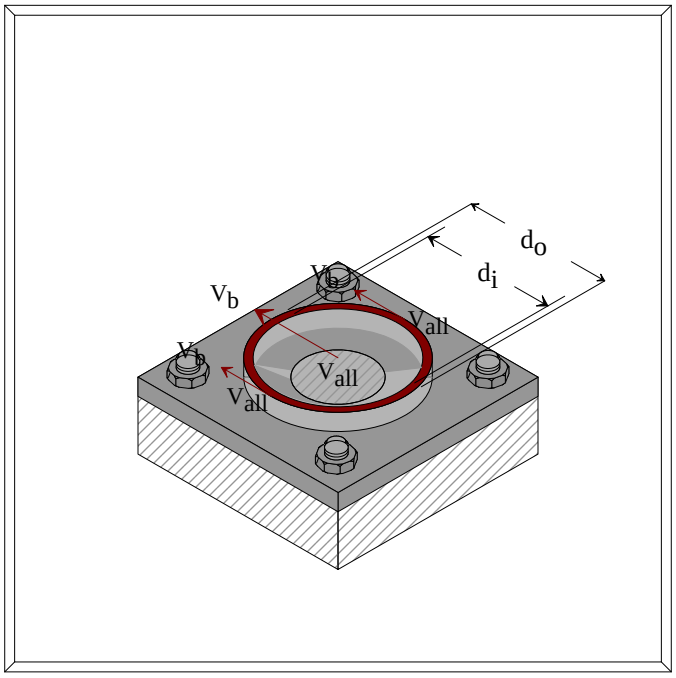

Figure 3.2.4.1

Substituting Equation 3.2.4.1

$$\tau_{all} = \frac{(V_{all} * Q_{max})}{(I_p * (d_o - d_i))} \qquad V_{all} = \tau_{all} * \frac{(I_p * (d_o - d_i))}{Q_{max}}$$

$$V_{all} = \tau_{all} * \frac{\left(\left(\frac{\pi}{64} * (d_o^{\,4} - d_i^{\,4})\right) * (d_o - d_i)\right)}{\left(\left(\frac{1}{12}\right) * (d_o^{\,3} - Di^{\,3})\right)} \qquad V_{all} = \tau_{all} * \frac{\left(\frac{3}{16} * \pi * (d_o^{\,4} - d_i^{\,4}) * (d_o - d_i)\right)}{(d_o^{\,3} - Di^{\,3})} \qquad \text{Eq. 3.2.4.2}$$

Letting...
d_o = 8 in.

d_i = 7.25 in

$$T_{all} = 4.50 * \tau_{all}$$ ---------- Eq. 3.2.4.3

Equation 3.2.4.3 states that given an allowable shear stress, the pole could support **4.50 lbs** of shear load for each available psi of bolt material strength.

3.3 Analysis of Shear Coupling

3.3.1 Shear Coupling: Allowable Bending Moment

The applied bending moment to the shear coupling is shown in Figure 3.3.1.1.

A short segment of the attached vertical pole is shown to emphasize the additional stiffness provided to the top octagon plate within the coupling due to the presence of the welded pole.

The top octagon plate of the assembly is assumed to rotate about an axis, some distance **h** from the center of the assembly. While not known, the dimension **h** is certainly greater than zero, but less than $\mathbf{R_m}$.

Assuming the stiffness of the top octagon plate and welded pole assembly is large compared to the axial stiffness of the edge caps vertical web, a linear variation of edge cap vertical web normal stress would appear reasonable.

It is assumed that the normal stress in the outer edge cap web has reached the allowable normal stress σ_{all}, and then varies in a linear manner to zero at the assumed bending axis **h** distance from the center.

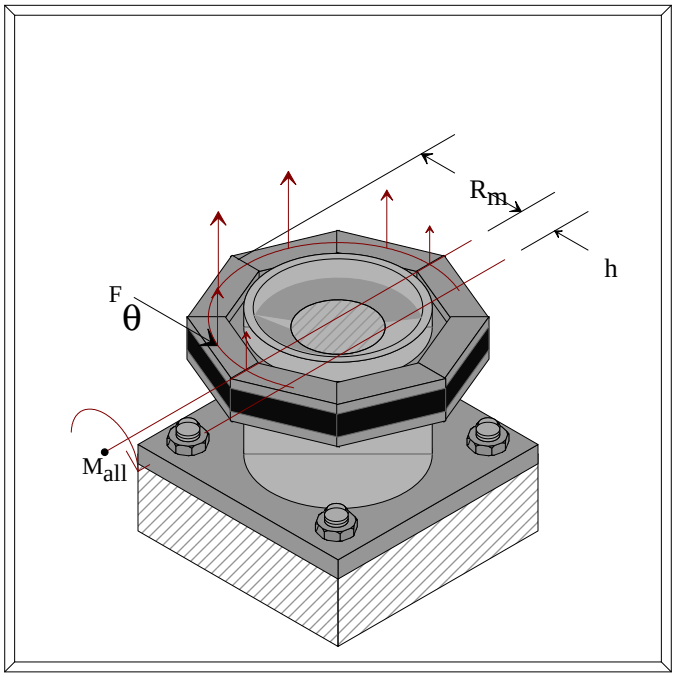

Figure 3.3.1.1

This geometry is clarified in the top planar projection of the coupling shown in Figure 3.3.1.2.

The normal stress region in the vertical web of the outer caps is assumed circular of mean radius $\mathbf{R_m}$ and thickness $\mathbf{W_t}$.

The variation of the normal stress, shown in the right portion of Figure 3.3.1.2, varies from the allowable stress σ_{all} at θ = 0 to zero at the assumed rotation axis **A-B**.

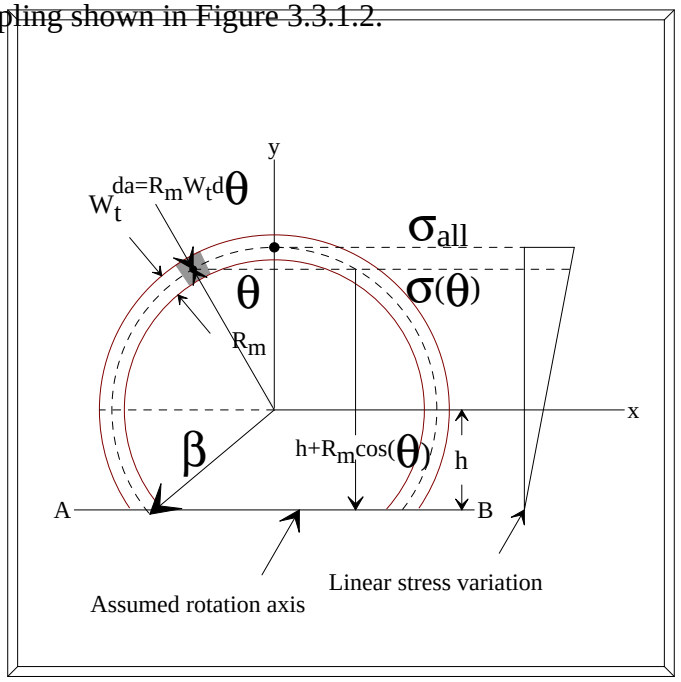

Figure 3.3.1.2

$$\sigma_\theta = \frac{(h + R_m * \mathrm{Cos}(q))}{(R_m + h)} * \sigma_{all}$$

The sum of moments due to this stress distribution is equated to the allowable bending moment **M_{all}**.

$$M_{all} = 2 * \int_0^{\pi/2+\beta} \frac{(h + R_m * \mathrm{Cos}(q))}{(R_m + h)} * \sigma_{all} * (h + R_m * \mathrm{Cos}(q)) * W_t * R_m * d\theta \quad \text{Eq. 3.3.1.1}$$

$$M_{all} = \frac{(2 * \sigma_{all} * R_m * W_t)}{(R_m + h)} * \int_0^{\pi/2+\beta} (h + R_m * \mathrm{Cos}(q))^2 * d\theta \quad \text{Eq. 3.3.1.2}$$

$$M_{all} = \frac{(2 * \sigma_{all} * R_m * W_t)}{(R_m + h)} * \int_0^{\pi/2+\beta} \left[h^2 + 2 * h * R_m * \mathrm{Cos}(q) + R_m^2 * \mathrm{Cos}^2(q)\right] * d\theta \quad \text{Eq. 3.3.1.3}$$

$$M_{all} = \frac{(2 * \sigma_{all} * R_m * W_t)}{(R_m + h)} * \int_0^{\pi/2+\beta} h^2 * d\theta$$

$$\frac{(\sigma_{all} * R_m * W_t)}{(R_m + h)} * \int_0^{\pi/2+\beta} 2 * h * R_m * \mathrm{Cos}(q) * d\theta$$

$$\frac{(\sigma_{all} * R_m * W_t)}{(R_m + h)} * \int_0^{\pi/2+\beta} R_m^2 * \mathrm{Cos}^2(q) * d\theta \quad \text{Eq. 3.3.1.4}$$

$$M_{all} = \frac{(2 * \sigma_{all} * R_m * W_t)}{(R_m + h)} * h^2 * q \Big|_0^{\pi/2+\beta}$$

$$\frac{(\sigma_{all} * R_m * W_t)}{(R_m + h)} * 2 * h * R_m * \mathrm{Sin}(q) \Big|_0^{\pi/2+\beta}$$

$$\frac{\left(\sigma_{all} * R_m * W_t\right)}{\left(R_m + h\right)} * R_m^{\,2} * \left(\frac{q}{2} + \operatorname{Sin}\left(\frac{2 * q}{2}\right)\right) \Bigg|_0^{\pi/2+\beta} \quad \text{---------- Eq. 3.3.1.5}$$

$$M_{all} = \frac{\left(2 * \sigma_{all} * R_m * W_t\right)}{\left(R_m + h\right)} * \left[\left(\frac{\pi}{2} + \beta\right)^2 + 2 * h * R_m * \operatorname{Sin}\left(\frac{\pi}{2} + \beta\right) + \frac{R_m^{\,2}}{2} * \left(\frac{\pi}{2} + \beta\right) + \frac{R_m^{\,2}}{2} * \operatorname{Sin}\left(\pi + 2 * \beta\right)\right]$$

Letting...
R_m = 6.25 in.

W_t = 0.5 in.

h = 4 in. (For h = 4)...β = $\operatorname{Tan}^{-1}(4/6.25)$ = **0.5693** radians

The above equation evaluates to...

$$M_{all} = 19.19 * \sigma_{all} \quad \text{---------- Eq. 3.3.1.6}$$

Equation 3.3.1.6 states that given an allowable normal stress, the coupling could support **19.19 in-lbs** of moment for each available psi of material strength.

3.3 Analysis of Shear Coupling

3.3.2 Shear Coupling: Allowable Normal Force

The applied normal force at the center of the shear coupling is shown in Figure 3.3.2.1

A short segment of the attached vertical pole is shown to emphasize the additional stiffness provided to the top octagon plate within the coupling due to the presence of the welded pole.

The applied normal force is equilibrated by a uniform distributed normal stress in the edge caps vertical web. The effective area is assumed to a mean radius R_m and a mean thickness W_t of the edge cap web.

$$N_{all} = A_c * \sigma_{all}$$

the area of the edge cap vertical web is assumed as...

$$A_c = 2 * \pi * R_m * W_t$$

Nall=2*p*Rm*Wt*sall Letting...

R_m = 6.25 in.

W_t = 0.5 in

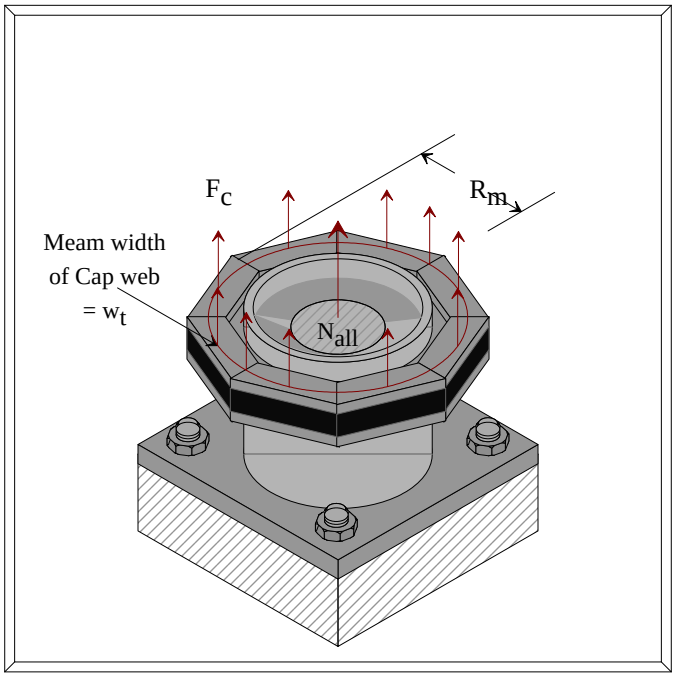

Figure 3.3.2.1

The allowable normal force from Equation 3.3.2.1 would be...

$$N_{all} = 19.63 * \sigma_{all} \quad \text{---------- Eq. 3.3.2.1}$$

Equation 3.3.2.2 states that given an allowable normal stress, the pole could support **19.63 lbs** of upward axial load for each available psi of material strength.

3.3 Analysis of Shear Coupling

3.3.3 Shear Coupling: Allowable Torsion

Two methods of supporting the applied torsion are presented.

Method 1

This method, presented in **Section 3.3.3.1**, utilizes the pre-tension in the binding straps to restrict the rotation of the top octagon plate relative to the bottom octagon plate.

Method 2

This method, presented in **Section 3.3.3.2**, utilizes a single notch placed along the center of one of the octagon edges. Both the top and bottom octagon plates are notched, the mating edge cap acting as a **double shear** torsional key. This method provides additional allowable torque when superimposed upon **Method 1**.

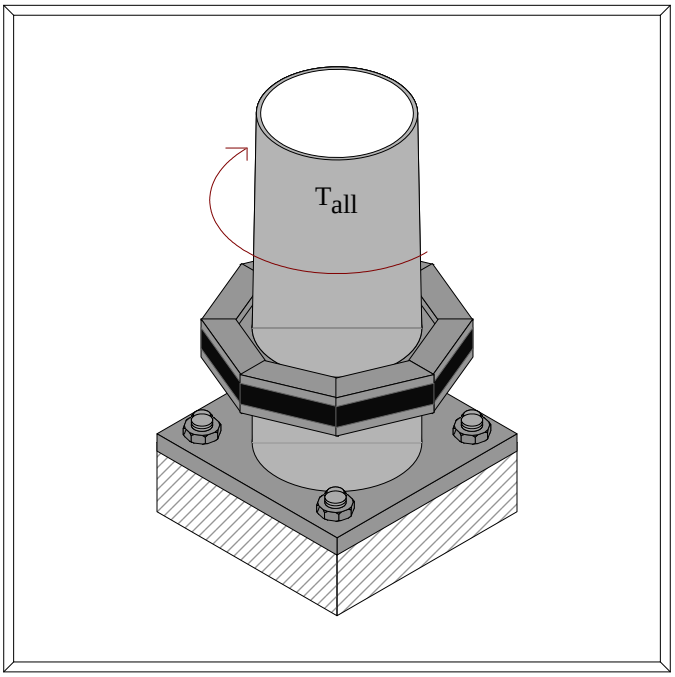

Figure 3.3.3.1

3.3.3 Analysis of Shear Coupling

3.3.3.1 Torsion Supported by Binding Strap

The applied torque at the center of the pole is shown in Figure 3.3.3.1.1 as applied to the center of the top octagon plate of the **Shear Coupling**.

The bearing stress σ_b between the edges of the octagon plates and the inner surfaces of each vertical web edge cap is shown applied to each surface of the octagon plates.

The bearing stress σ_b is adjusted with the pre-tension in the steel strap used to retain the edge caps.

As a torque is applied, the top octagon plate attempts to rotate with respect to the bottom octagon plate. This attempted rotation is exaggerated in Figure 3.3.3.1.1.

To initiate this rotation, each corner of the top octagon plate attempts to lift and rotate each edge cap about it's adjacent corner. These **8** individual forces **P**, shown in Figure 3.3.3.1.1, act through the moment level arm **$(1/2)L_{pe}$** to equilibrate the applied torque **T_{all}**.

$$T_{all} = 8 * P * \frac{L_{pe}}{2} \qquad \text{Eq. 3.3.3.1.1}$$

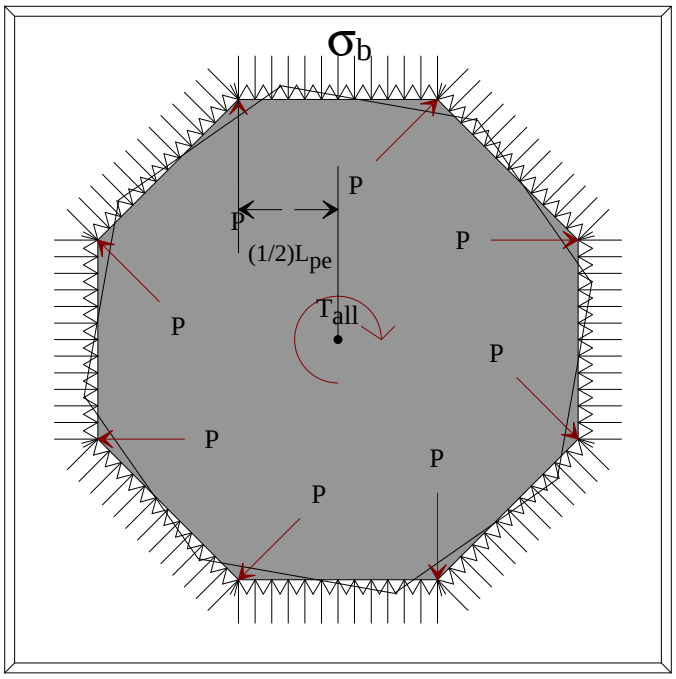

Figure 3.3.3.1.1

Taking the moments about a typical adjacent edge cap corner...

$$P * L_{pe} - \sigma_b * L_{pe} * t_p * \left(\frac{L_{pe}}{2}\right) = 0 \qquad \text{Eq. 3.3.3.1.2}$$

Solving for **P** and substituting into Equation 3.3.3.1.1...

$$T_{all} = 8 * \left(\sigma_b * t_p * \left(\frac{L_{pe}}{2}\right)\right) * \frac{L_{pe}}{2} \qquad T_{all} = 2 * \sigma_b * t_p * L_{pe}^{\,2} \qquad \text{Eq. 3.3.3.1.3}$$

The bearing stress between the octagon plate edges and the inner surface of the vertical web edge caps is adjusted with the tension or pre-stress of the steel retaining strap.

Consider Figure 3.3.3.1.2.

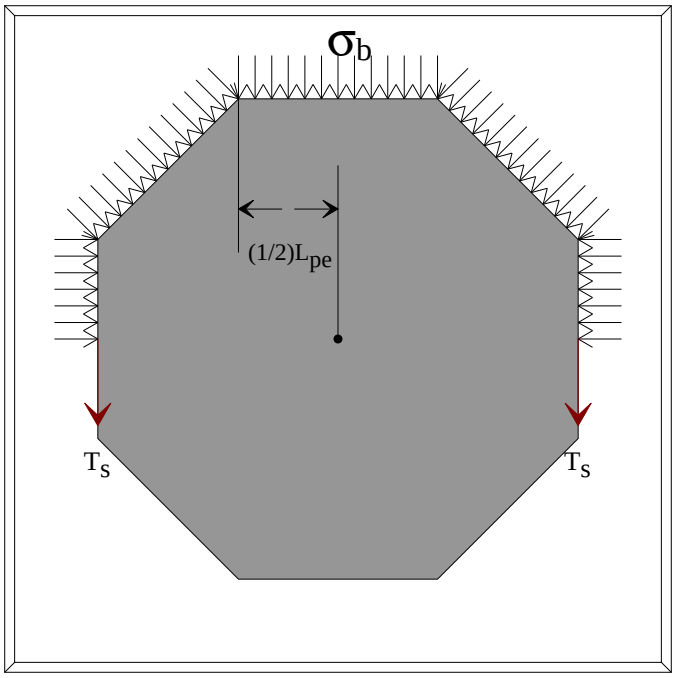

Figure 3.3.3.1.2

Summing vertical forces, the bearing stress σ_b created by the strap tension $\mathbf{T_s}$...

$$2 * T_s = 2 * \left[2 * L_{pe} * t_p * \sigma_b * \sin(45)\right] + 2 * L_{pe} * t_p * \sigma_b$$

$$T_s = L_{pe} * t_p * \sigma_b * \left(2 * \sin(45) + 1\right)$$

$$\sigma_b = \frac{T_s}{L_{pe} * t_p * \left(2 * \sin(45) + 1\right)}$$

-----Eq. 3.3.3.1.4

Substituting Equation 3.3.3.1.4 into Equation 3.3.3.1.3...

$$T_{all} = 2 * \sigma_b * t_p * L_{pe}^2$$

$$T_{all} = 2 * \left(\frac{T_s}{L_{pe} * t_p * \left(2 * \sin(45) + 1\right)}\right) * t_p * L_{pe}^2$$

$$T_{all} = 2 * L_{pe} * \frac{T_s}{2 * \mathrm{Sin}(45) + 1}$$

$$T_{all} = 0.8284 * L_{pe} * T_s$$ ---------- Eq. 3.3.3.1.5

Letting...
L_{pe} = 4.592 in.

$$T_{all} = 3.804 * T_s$$ ---------- Eq. 3.3.3.1.6

Equation 3.3.3.1.6 suggests that for each 1000 lbs. of strap pre-tension, **3804 in-lbs**, or **317 ft-lbs** of applied torsion may be resisted. Stainless steel strapping band tension loads of up to 7000 lbs are available. This would provide up to 2200 ft-lbs of applied torsion. The code requirements for this case must be reviewed, but this level of torsional resistance seems adequate.

Note:

This conclusion is thought to be very conservative. Once the edge caps begin to rotate, the geometry of how the adjacent edge caps interact is a bit awkward. The necessary assumptions to mathematically model the interaction is also debatable. However, the author's intuition is that the edge caps will lock-up and support considerably more torque than this initial phase predicts. The mathematics to support this opinion has not been created. While this **locking** feature may exist, it would not be good engineering practice to depend upon this feature since torsional loading would most probably be due to buffeting wind loads. Such repeative loads could cause a deterioration of the **Shear Coupling** assembly.

3.3 Analysis of Shear Coupling

3.3.3.2 Shear Supported by a Single Octagon Edge Notch

An **alternate solution** would be to notch both octagon plates along one edge, and use one mating edge cap as a torsional key. The assembly with the edge caps removed is shown Figure 3.3.3.2.1.

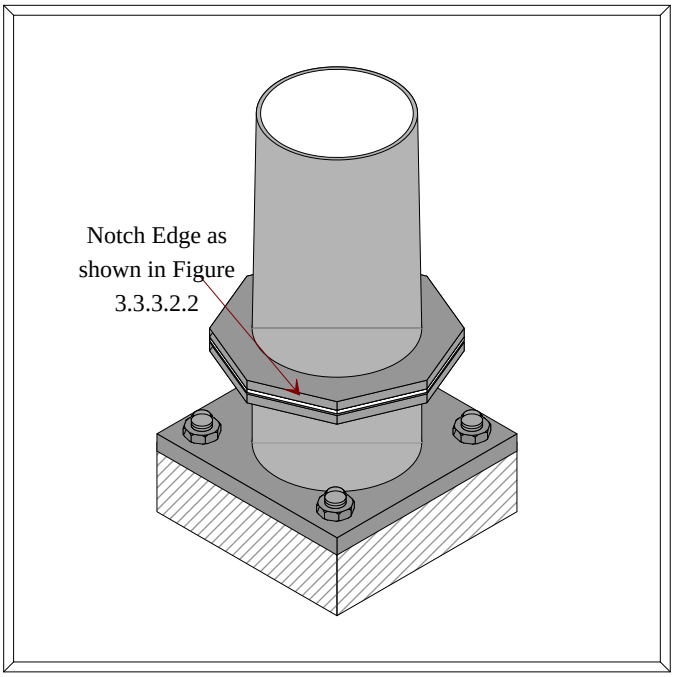

Figure 3.3.3.2.1

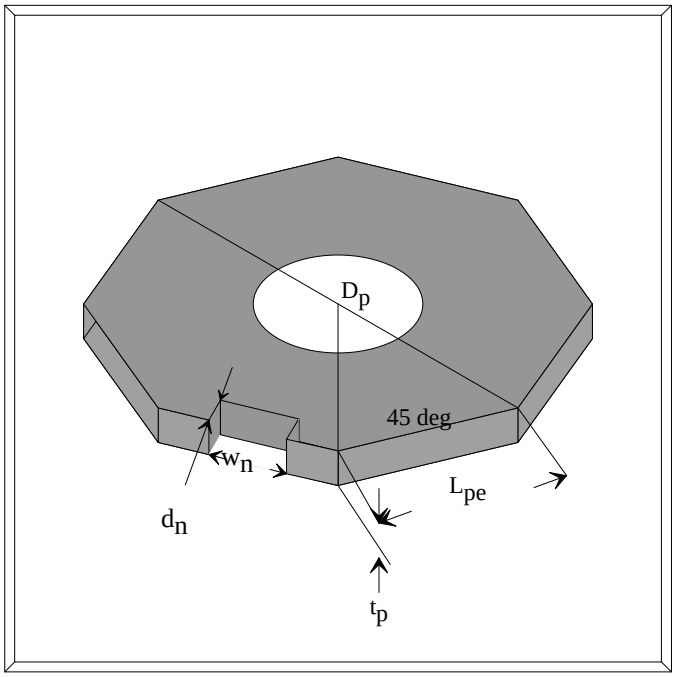

Figure 3.3.3.2.2

The details of the notch in one of the octagon plates is shown in Figure 3.3.3.2.2.

For the generic pole of this analysis, the width of the symmetric notch is assumed to be... $\mathbf{w_n = 2"}$ along the $\mathbf{L_{pe} = 4.592"}$ edge length,

and the depth as $\mathbf{d_n = 1"}$. This provides a shear area of $\mathbf{A_s = 2}$ in^2. The lever arm $\mathbf{L_p}$ is computed as...

$\mathbf{L_n = 5.543"}$.

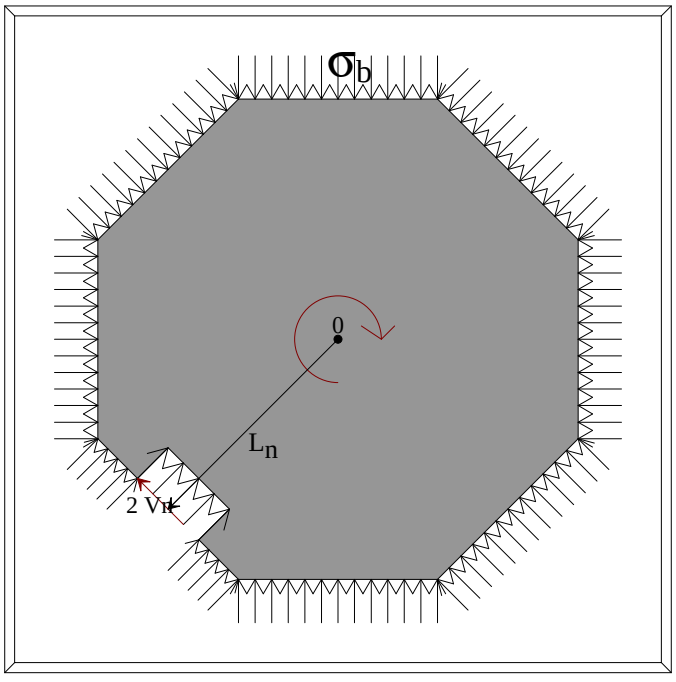

Figure 3.3.3.2.3

Equilibrating the **double shear** shear force $\mathbf{2V_n}$ to the applied torque T_{all}...

$$2 * V_n * Lp = T_{all} \qquad T_{all} = 2 * A_s * Lp * \tau_{all}$$

$$T_{all} = (2) * (2) * (5.543) * \tau_{all} \qquad T_{all} = 22.18 * \tau_{all} \qquad \text{Eq. 3.3.3.2.1}$$

Equation 3.3.3.2.1 states that given an allowable shear stress, the **Shear Coupling** could support **22.18 in-lbs** of applied torque for each available psi of material strength.

Since the notch is rectangular, the horizontal shear separation characteristics of the **Shear Coupling** would no longer be **Omni-directional**. This would suggest a preferred impact zone as shown in Figure 3.3.3.2.4.

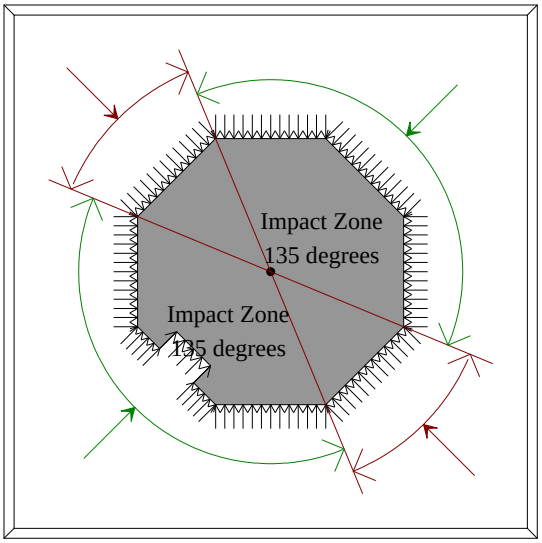

Figure 3.3.3.2.4

As the impact angle approached the limits of the impact zone the **Shear Coupling** would still separate, but at much higher loads. While these higher loads may still be within acceptable crashworthy limits, the probability of damage to the octagon plates and keyed edge cap increases, thus defeating one of the primary advantages of re-setting the pole without repair.

A slight change in the geometry of both the top and bottom octagon plate notch may minimize this possible damage and re-establish the desired **Omni-directional** nature of the assembly.

The geometry of the notch is modified as shown in Figure 3.3.3.2.5.

Upon impact the binding strap elongates, the top plate translates, un-seating the edge cap key from the top plate.

The slight taper in the notch now permits unrestricted top plate rotation.

This sequence is shown in Figure 3.3.3.2.5.

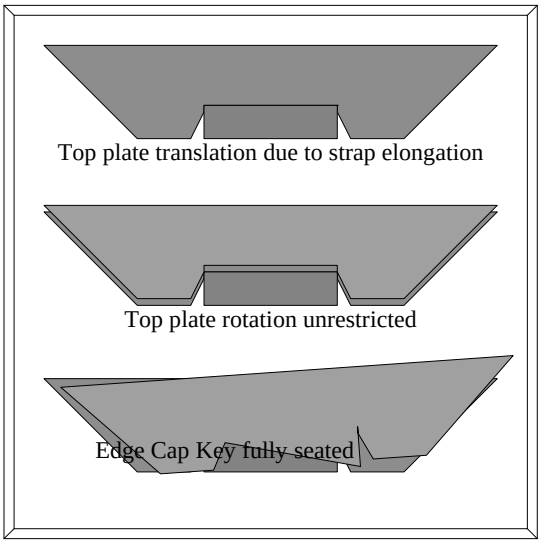

Figure 3.3.3.2.5

In this case, however, the edge cap key is closer to a very short beam with an applied end load than a double shear key. An approximation of this maximum shear stress would be...

$1.5(V_n/A_s)$ with an adjustment of $\mathbf{L_n}$ in Figure 3.3.3.2.3 to $\mathbf{L_n}$ = **4.543"**.

$$T_{all} = V_n * L_n$$

$$\tau_{all} = 1.5 * \frac{V_n}{A_s}$$

$$V_n = \frac{(A_s * \tau_{all})}{1.5}$$

$$T_{all} = \left(\frac{(A_s * \tau_{all})}{1.5}\right) * L_n \qquad T_{all} = \left(\frac{(2.0 * \tau_{all})}{1.5}\right) * (4.543)$$

$$T_{all} = 6.06 * \tau_{all}$$ ---------- Eq. 3.3.3.2.2

Equation 3.3.3.2.2 states that given an allowable shear stress, the **Shear Coupling** could support **6.06 in-lbs** of applied torque for each available psi of material strength.

These results are further discussed in Section 3.3.4.

3.3 Analysis of Shear Coupling

3.3.4 Shear Coupling: Allowable Shear Force

The applied horizontal shear is assumed at the center of the pole and is shown in Figure 3.3.4.1.

The bearing stress σ_b between the edges of the octagon plates and the inner surfaces of each vertical web edge cap due to pre-tension of the steel strap is also shown in the figure. In the absence of any horizontal shear, this bearing stress distribution will be uniform both around the perimeter of the octagon as well as the top and bottom plates.

As a shear is applied, the top octagon plate attempts to slide with respect to the bottom octagon plate. This attempted horizontal relative motion is exaggerated in Figure 3.3.4.1.

This relative motion causes the bearing stresses to become non-uniform. Horizontal force equilibrium must now be shared between the applied shear, pre-stress strap tension, and the pre-set bearing stresses on both the top and bottom octagon plates.

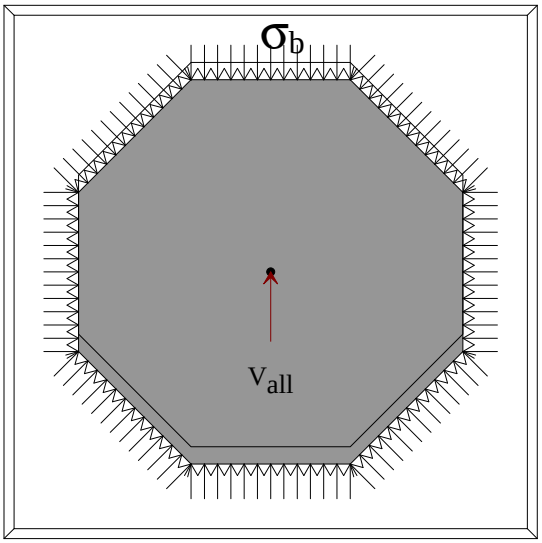

Figure 3.3.4.1

As the top plate moves Δ**p**, the bearing stresses between the top and bottom plates change as exaggerated in Figure 3.3.4.2. As $\mathbf{V_{all}}$ is increased, Δ**p** increases, shown as upward motion of the top plate in the figure. The top plate edge **A-B** will separate from its edge cap, and the bottom plate edge **C-D** will separate from its edge cap.

This separation is denoted by the bearing stress on these edges approaching zero. The applied horizontal shear causing this condition is considered the limit or allowable shear $\mathbf{V_{all}}$.

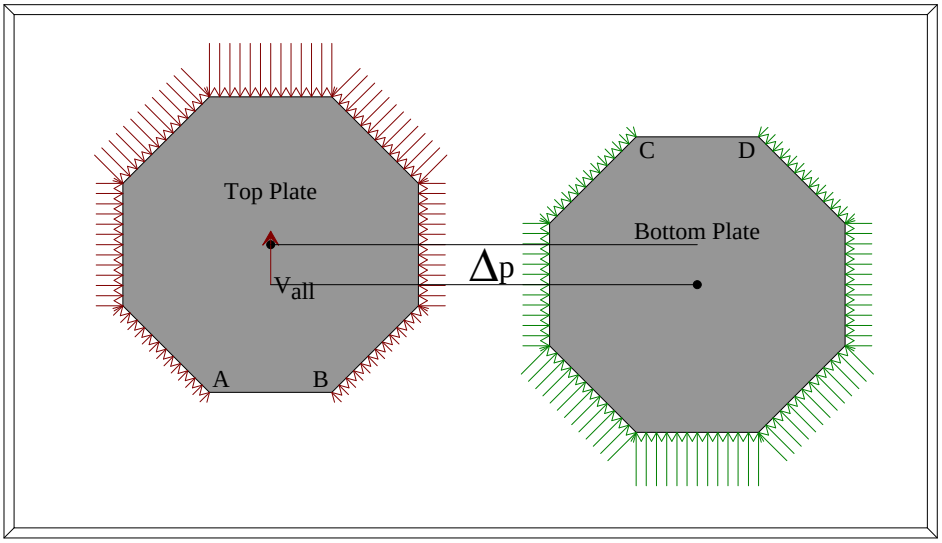

Figure 3.3.4.2

Recall from Section 3.3.3, that a pre-tension in the strap $\mathbf{T_S}$ was used to control the allowable torsion $\mathbf{M_{all}}$. This pre-tension $\mathbf{T_S}$ shorten the original length of the strap by...

$$\Delta_{L_S} = -\frac{(T_S * L_S)}{(A_S * E_S)} \qquad \text{Eq. 3.3.4.1}$$

If there were no pre-tension and horizontal shear load applied, the tension in the steel strap would be $\mathbf{(1/2)V_{all}}$. This strap tension would elongate the steel strap by...

$$\Delta_{L_S} = \frac{\left(\frac{V_{all} * L_S}{2}\right)}{(A_S * E_S)} \qquad \text{Eq. 3.3.4.2}$$

Superimposing Equation 3.3.4.1 and Equation 3.3.4.2...

$$0 = -\frac{(T_S * L_S)}{(A_S * E_S)} + \frac{\left(\frac{V_{all} * L_S}{2}\right)}{(A_S * E_S)} \qquad \text{Eq. 3.3.4.3}$$

Canceling terms, the allowable shear $\mathbf{V_{all}}$ becomes...

$$V_{all} = 2 * T_S \qquad \text{Eq. 3.3.4.4}$$

The superposition of the bearing stresses of Figure 3.3.4.2 are self-equilibrating. The application of a horizontal shear will further increase the strap tension above the pre-tension level, and begin to elongate the already shortened strap until the strap returns to its original length. It is at this level that any addition horizontal shear will begin to separate the upper and lower octagon plates from their respective edge caps.

For applied horizontal shear below the level of Equation 3.3.4.4, no relative plate motion occurs. The internal bearing stresses between the top and bottom plates of the **Shear Coupling** are adjusted to remain self-equilibrating and to support the applied shear.

The implications of Equation 3.3.4.4 will help establish the load-deflection characteristics of **Shear Coupling** and significantly affect the dynamic analysis.

3.4 Summary of Analysis

The results of the static stress analysis of the **Shear Coupling** presented in Sections 3.1, 3.2, and 3.3 are summarized.

Recall that the comparative analysis approach used the allowable normal and shear stresses as a means of comparing the generic pole **Shear Coupling** to that of the pole and pole support base. The pole and pole support base already meet all code requirements.

Also recall that the **Shear Coupling** has been dimensionally set with reference to the pole base so that conclusions drawn for this generic pole apply to any other pole, be it larger or smaller, as long as it is supported by a four bolt base pattern.

Allowable	Pole base	Pole	Shear Coupling
Bending Moment	$M_{all} = 16.49 * \sigma_{all}$	$M_{all} = 16.35 * \sigma_{all}$	$M_{all} = 19.19 * \sigma_{all}$
Normal Force	$N_{all} = 3.14 * \sigma_{all}$	$N_{all} = 8.89 * \sigma_{all}$	$N_{all} = 16.63 * \sigma_{all}$
Torsion Loads	$T_{all} = 19.98 * \tau_{all}$	$T_{all} = 32.72 * \tau_{all}$	$T_{all} = 3.804 * T_s$
Torsion Loads	Single Notch		$T_{all} = 22.18 * \tau_{all}$
Torsion Loads	Single Notch	(Modified)	$T_{all} = 6.06 * \tau_{all}$
Shear Loads	$V_{all} = 3.14 * \tau_{all}$	$V_{all} = 4.5 * \tau_{all}$	Vall=2*Ts

Comment on Allowable Bending Moment (see Table)

The pole base and pole are nicely balanced in design, **16.49 compared to 16.35**.

The **Shear Coupling** exceeds the design requirements being **19.19**.

Comment on Allowable Normal Force (see Table)

The pole is stronger than the pole base **8.89 compared to 3.14**.

The **Shear Coupling** doubles the design requirements being **16.63**.

Comment on Allowable Torsion (see Table)

The pole is stronger than the pole base **32.72 compared to 19.98**.

The **Shear Coupling** could not use the allowable shear stress τ_{all} as a comparative measure.

It depends upon the strap tension and would support **3.8 in-lbs** of torsion for each **lb** of strap tension. This translates into about **317 ft-lbs** of torsion per **1000 lbs** of strap tension. Obtaining up to **5000 lbs** of strap tension is possible, so this item would require a specific check with codes.

The impact zone is **Omni-directional**.

Comment on Allowable Torsion: Single Edge Notch (see Table)

Notching the octagon plates with a single edge notch provides a $T_{all} = 22.18*\tau_{all}$, which is greater than the base capability.

The impact zone is reduced to 135 degrees.

Comment on Allowable Torsion: Single Modified Edge Notch (see Table)

Notching the octagon plates with a single modified edge notch provides a $T_{all} = 6.06*\tau_{all}$, which is less than the base capability.

The impact zone is **Omni-directional**.

Comment on Allowable Shear (see Table)

The pole base and pole are nicely balanced in design, **3.14 compared to 4.5**.

Unfortunately, the **Shear Coupling** could not use the allowable shear stress τ_{all} as a comparative measure.

It also depends, upon the strap tension and would support **2 lbs** of horizontal shear for each **lb** of strap tension. Since the strap will certainly have a pre-tension to several thousand pounds, this item is not considered critical. Horizontal shear requirements are probably set for the horizontal earthquake component of a **1 G** or less quake, for which the **Shear Coupling** could readily qualify.

4.0 Dynamic Analysis: One-Dimensional Model

The crashworthy properties of the **Shear Coupling** was analyzed utilizing a simple one-dimensional model of the pole and an impacting vehicle.

The actual problem is more involved in that the motion of the pole after impact and separation is important. Clearly, the dynamic rotation and vertical motion of the pole and how the pole would interact with the vehicle after separation merits further analysis.

However, for the limited purpose of the separation characteristic of the **Shear Coupling**, and the velocity change imparted to the impacting vehicle, a one-dimensional analysis will suffice.

A simple model of the pole, **Shear Coupling**, and impacting vehicle is shown in Figure 4.0.1.

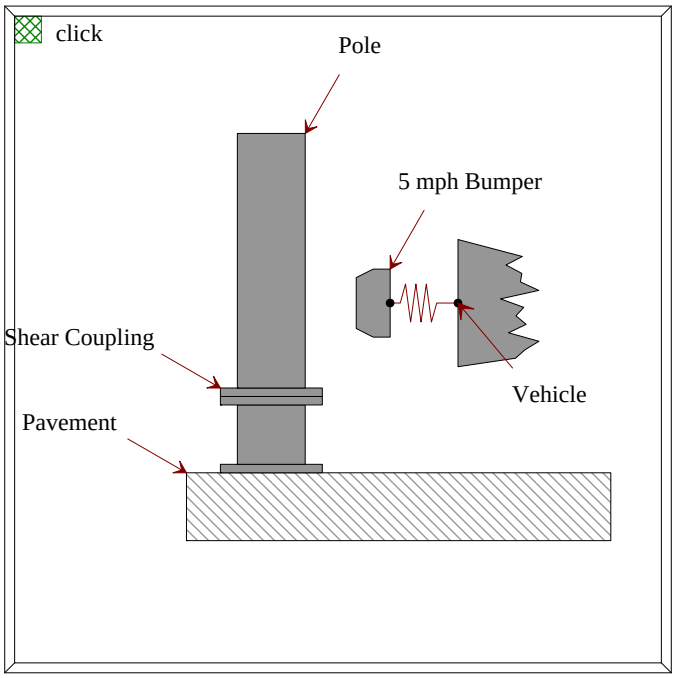

Figure 4.0.1

A mathematical model is shown in Figure 4.0.2.

Since the one-dimensional nature of the model requires an alignment of the **CG** of the vehicle and pole, results would be reasonably valid only during the short time between initial contact and pole separation. The **CG** of the pole system is actual well above the bumper contact point, however, the distance between the contact point and the shear coupler is small, the shear coupler being beneath the impacting vehicle's undercarrage. The resulting moment about the centroidal axis perpendicular to the plane of the pole in **Figure 4.0.2** would be small during this initial period of impact. As such, an insight into the significant kinematic features of the impact may be obtained from such an analysis.

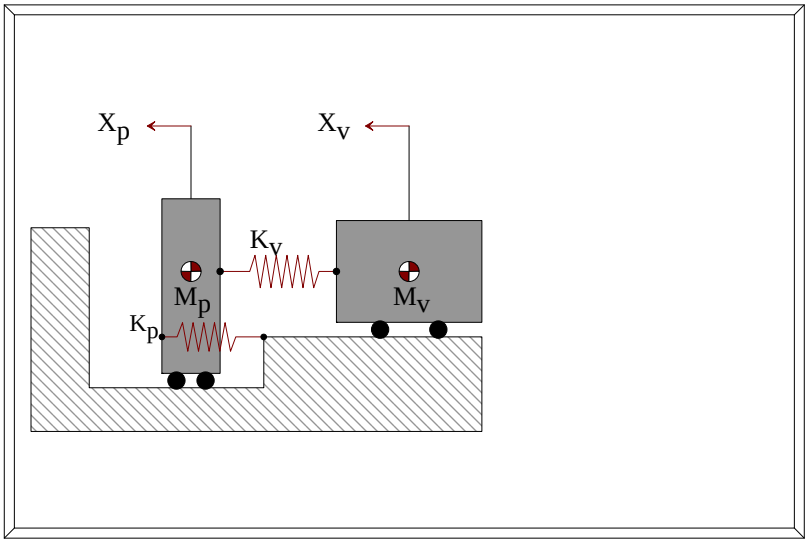

Figure 4.0.2

The mass of the pole and vehicle are denoted as **M_p** and **M_v** and the load deflection characteristics of the **Shear Coupling** and vehicle bumper are denoted as **K_c** and **K_b**.

Applying $\sum F = Ma$

$$M_v * \ddot{x}_v = -(X_v - X_p) * K_b$$

$$M_p * \ddot{x}_p = (X_v - X_p) * K_b - X_p * K_c \qquad \text{Eq. 4.0.1}$$

The shear coupler load-deflection characteristics

The load deflection characteristics of the shear coupler is directly controlled by the characteristics of the binding strap holding the edge caps in place.

For the purposes of this analysis we will assume a **1.5"** wide by **0.068"** thick high strength steel alloy strap pre-tensioned to **4000** lbs is to be used. The strap pre-tension of 4000 lbs would support approximately 1260 ft-lbs of applied torque to the pole at a pre-tension stress level of approximately **40,000** psi. (see Section 3.3.3.1).

As previously discussed, if a **2500** lb vehicle at **5** Mph strikes the pole, a **12,500** max force is required to bring the vehicle to rest. This additional 12,500/2 = **6,250** lb. strap load increases the strap tension to approximately **10,250** lbs, or a max tensile stress of 10,250/(1.5)(0.068) = **100.5** ksi. So, if, a high strength steel alloy capable of 125 ksi yield stress, 145 ksi ultimate stress, and **12%** elongation is used...

The strap elongation, as measured from the pre-tension state...

$$\Delta_{L_s} = \frac{(F_s * L_s)}{(A_s * E_s)}$$

$$d_c = 2 * \Delta_{L_s}$$

$$K_c = \frac{F_s}{d_c} = \frac{(A_s * E_s)}{(2 * L_s)}$$

$$K_c = \frac{(1.5 * 0.068 * 30E06)}{(2 * 18)} = 85000$$

Eq. 4.0.2

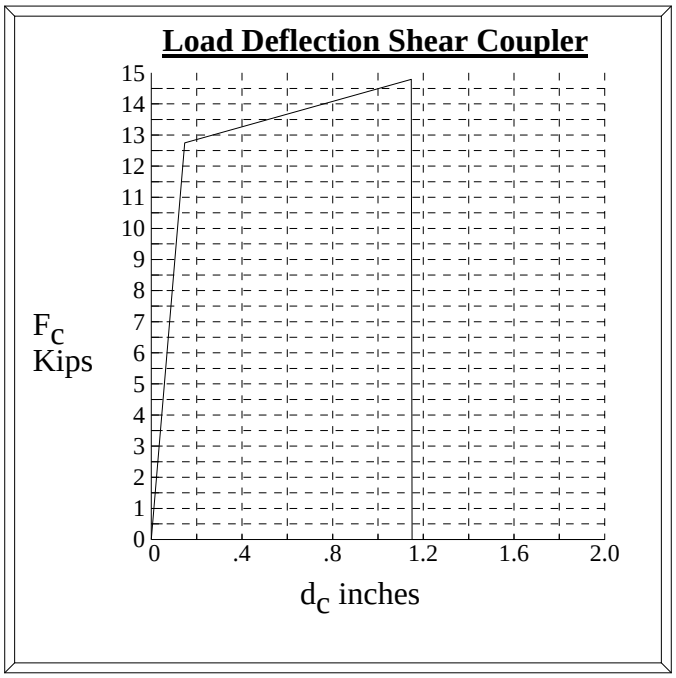

Figure 4.0.3

The effective spring constant for the shear coupler is assume to be **85,000** lb/in, up to a limit of an applied **12750** lbs, at which level the stress in the strap is **125,000** psi. a **12%** elongation then occurs for the **18** length of the strap before failure is assumed. The assumed load deflection curve is shown in **Figure 4.1.7**. The force **F_c** and deflection **d_c** of **Figure 4.1.7** is the resisting force provided by the shear coupler to pole motion as a function of the relative horizontal top plate motion.

The bumper load-deflection characteristics

Most vehicles advertise a bumper system which allows a front impact with a solid object at some low velocity which uopn bring the vehicle to rest results in no damage to the bumper system. The so called 5 mph elastic bumper.

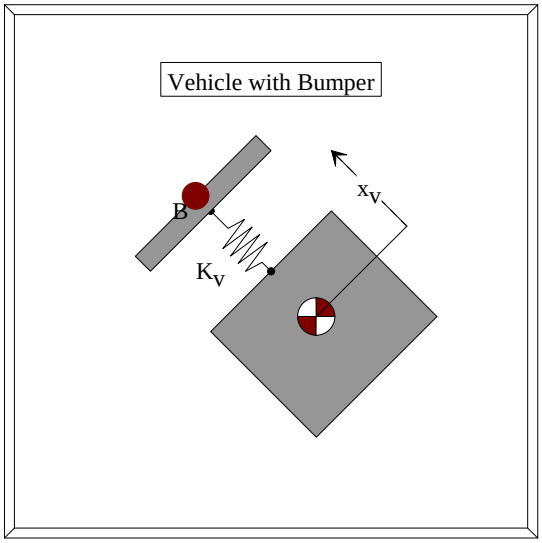

Figure 4.0.4

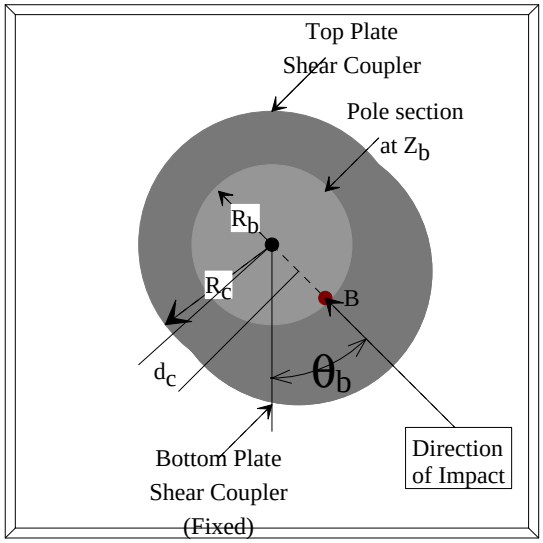

Figure 4.0.5

The load deflection characteristics of the front bumper of the impacting vehicle is assumed to be a typical 5 mph bumper with linear elastic characteristics of stroke ,$\mathbf{d_b}$ inches followed by an increased load deflection slope beyound the $\mathbf{d_b}$ stroke limit. This increased loading slope is assumed to be of an order of magnitude of 10 times stiffer than the elastic section. A near vertical unloading slope is used to permitting the vehicle to separate from the pole, if the kinematics requires, resulting a completely plastic deformation of the vehicle beyound the initial $\mathbf{d_b}$ elastic limit. These characteristics are developed for a range of vehicle weights, and while certainly subject to debate, do indeed provide a starting point to investigate the pole kinematics due to a vehicle impact.

The elastic energy absorbed by a bumper in an assumed $\mathbf{d_B}$ distance would be $1/2F_Bd_B$ in-Lbs where F_B is the max force in Lbs supported by the bumper. This energy is equated to the kinetic energy of a vehicle of weight $\mathbf{W_V}$ Lbs moving a velocity $\mathbf{V_V}$ in/sec., or $1/2M_VV_V^2$ in-Lbs.

$$\frac{1}{2} * d_B * F_B = \frac{1}{2} * \frac{W_V}{g} * \left(V_V\right)^2 \quad \text{Eq. 4.0.3}$$

solving for the max force F_B...

$$F_B = \frac{W_V}{\left(g * d_B\right)} * \left(V_V\right)^2 \quad \text{Eq. 4.0.4}$$

Thus the assumed elastic slope, plastic slope, and unloading slopes become...

$$S_{B1} = \frac{F_B}{d_B}$$

$$S_{B2} = 10 * \frac{F_B}{d_B}$$

$$S_{B3} = 100 * \frac{F_B}{d_B} \qquad \text{----------Eq. 4.0.5}$$

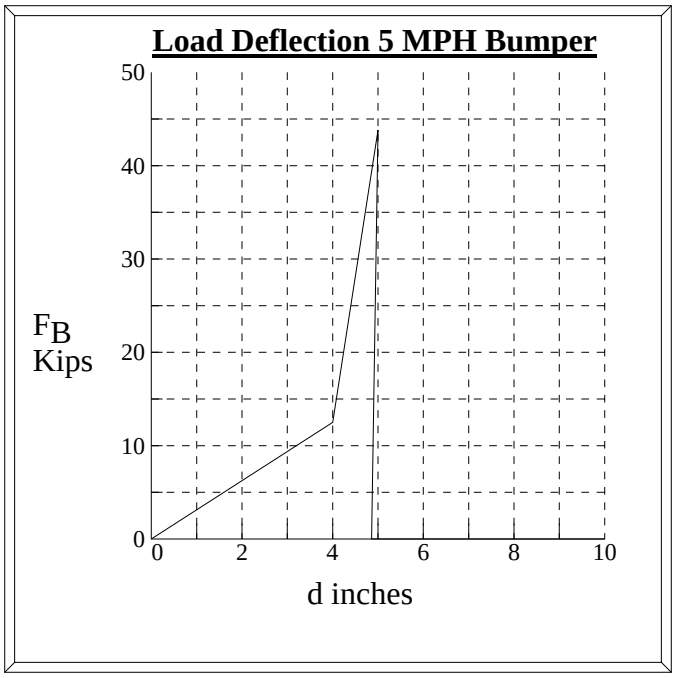

Figure 4.0.6

These characteristics are shown in **Figure 4.1.6** for a **2500** Lbs vehicle with a **5 Mph** (88 in/sec) **4 in** stroke elastic bumper.

$$F_B = \frac{W_v}{(g * d_B)} * (V_v)^2 = 12538$$

$$S_{B1} = \frac{F_B}{d_B} = 3134$$

$$S_{B2} = 10 * \frac{F_B}{d_B} = 31340 \qquad \text{---------- Eq. 4.0.6}$$

$$S_{B3} = 100 * \frac{F_B}{d_B} = 313400$$

The One dimensional solution

The equation set **Eqs.4.0.1** is repeated here, with the initial conditions of...

$$M_v * \ddot{x}_v = -(X_v - X_p) * K_b$$

$$M_p * \ddot{x}_p = (X_v - X_p) * K_b - X_p * K_c \qquad \text{----------Eq. 4.0.7}$$

at time =0, the displacements of the vehicle and pole are zero, and the velocity of pole is zero, and the velocity of the vehicle is $\dot{x}_v$. At time zero, the vehicle bumper is just touching the pole.

$x_v(0) = 0$, and $x_p(0) = 0$
$\dot{x}_v(0) = 88$, and $\dot{x}_p(0) = 0$

A **2500** lbs vehicle impact at 4, 6, 8, and 10 mph, (70.4, 88, 140.8, and 176) in/sec was obtained using a fourth order Runga-Kutta method. A time step 0f **0.0001 sec** was used, with data stored every **0.001 sec**.

The vehicle velocity time history is shown in **Figure 4.0.7**

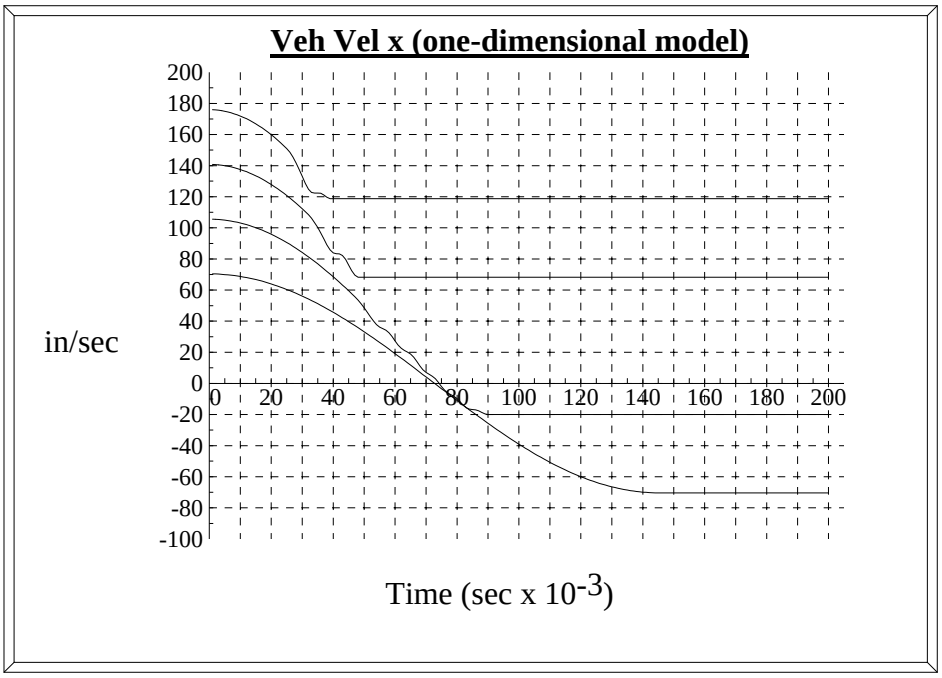

Figure 4.0.7

Figure 4.0.7 has some interesting features.
4 Mph impact (Black/Bottom curve): The initial impact velocity is **70** in/sec and the final velocity is **-70** in/sec. This suggest a fully elastic rebound with no damage to the vehicle. The shear coupler has not separated.
6 Mph impact (Red/second from Bottom Curve): The initial impact velocity is **106** in/sec in/sec and the final velocity is **-18** in/sec. This suggest a vehicle rebound with some eneryg absorbed due to plastic deformation of the bumper. elastic rebound with no damage to the vehicle. The shear coupler has not separated.

8 Mph impact (Green/second from Top Curve): The initial impact velocity is **141** in/sec and the final velocity is **24** in/sec. This suggest the vehicle impact failed the shear coupler, energy having been absorbed, resulting in a velocty change of **117** in/sec, with the vehicle continuing in the same direction at the reduced velocity of **24** in/sec.
10 Mph impact (Blue/Top Curve): The initial impact velocity is **176** in/sec and the final velocity is **80** in/sec. This suggest the vehicle impact failed the shear coupler, energy having been absorbed, resulting in a velocty change of **96** in/sec, with the vehicle continuing in the same direction at the reduced velocity of **80** in/sec.

The Pole velocity time history is shown in **Figure 4.0.8**

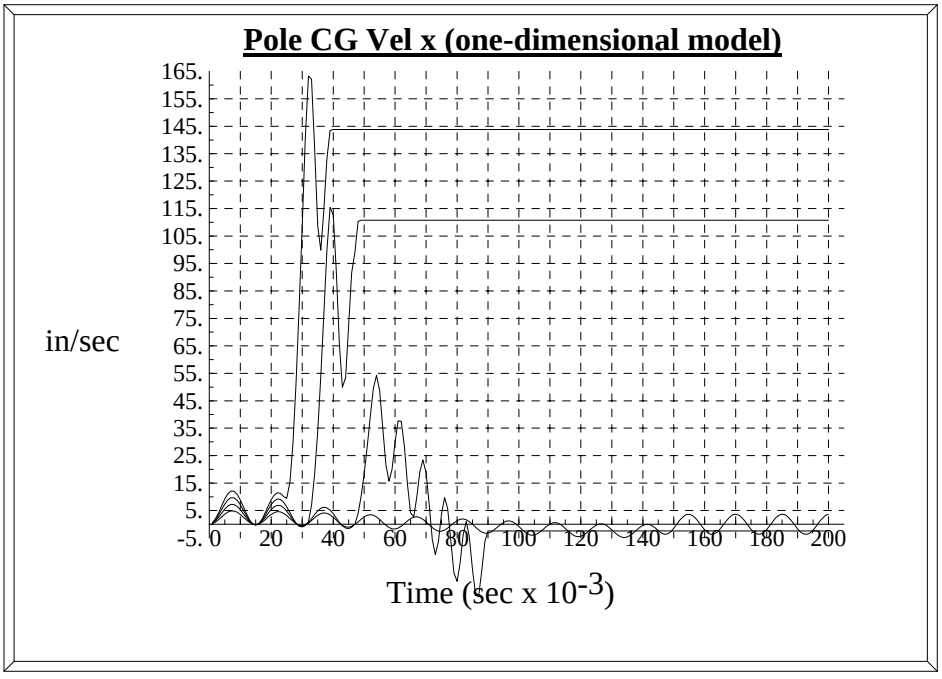

Figure 4.0.8

Figure 4.0.8 has some interesting features.
4 Mph impact (Black/Bottom curve): Although a difficult to see, the velocity of the pole cg oscillates between + and - **5** in/sec. The coupler does not fail and in fact is not damaged. The spring force time-history is not shown for the coupler, but it remains elastic. Notice in this case, that the vehicle and pole has both been undamaged.
6 Mph impact (Red/second from Bottom Curve): The oscillation of the pole relative velocity is due to the natural frequency of the pole. The spring force time-history is not shown for the coupler, but it enters the plastic region but does not completely fail, thus the pole oscillates but returns to a zero velocity. The coupler has been damaged and would need to be replaced. Notice in this case, that the vehicle and pole has both been damaged but the pole remains standing.

8 Mph impact (Green/second from Top Curve): The shear coupler fails at approximately **40-50** milli-seconds, separates from the vehicle and has a velocity of **75** in/sec. The important point being that the pole separation velocity (**75** in/sec) is greater than the resulting vehicle velocity (**24** in/sec) from **Figure 4.0.7** by a positive relative velocity of **51** in/sec.
10 Mph impact (Blue/Top Curve): The shear coupler fails at approximately **30-40** milli-seconds, separates from the vehicle and has a velocity of **150** in/sec. The important point being that the pole separation velocity (**150** in/sec) is greater than the resulting vehicle velocity (**80** in/sec) from **Figure 4.0.7** by a positive relative velocity of **70** in/sec.

Conclusion to this one-dimensional analysis An important feature is predicted by this one-dimensional analysis. The high strength steel alloy strap binding the shear coupler caps together store a great deal of elastic energy as the coupler begins to fail. This elastic energy, along with the elastic energy of the vehicle bumper being simulaneously released at failure of the coupler accelerates the pole cg forward producing a positive velocity of the pole cg relative to that the vehicle. In simpler terms, the coupler failure literally catapults the pole forward.

It is important to understand the value of this simple analysis. A three dimensional view of this one-dimensional analysis is shown in **Figure** 4.0.9. The above conclusions apply about 40-50 milli-seconds after impact.The top plate of the failed coupler having moved horizontally about **1** inch, but still being supported vertically by the bottom plate of the coupler. Its horizontal velocity being between **25 to 80** in/sec will move the pole horizontally an additional **2** inches, thus clearing the bottom plate of the coupler, in less and 100 milli-seconds.

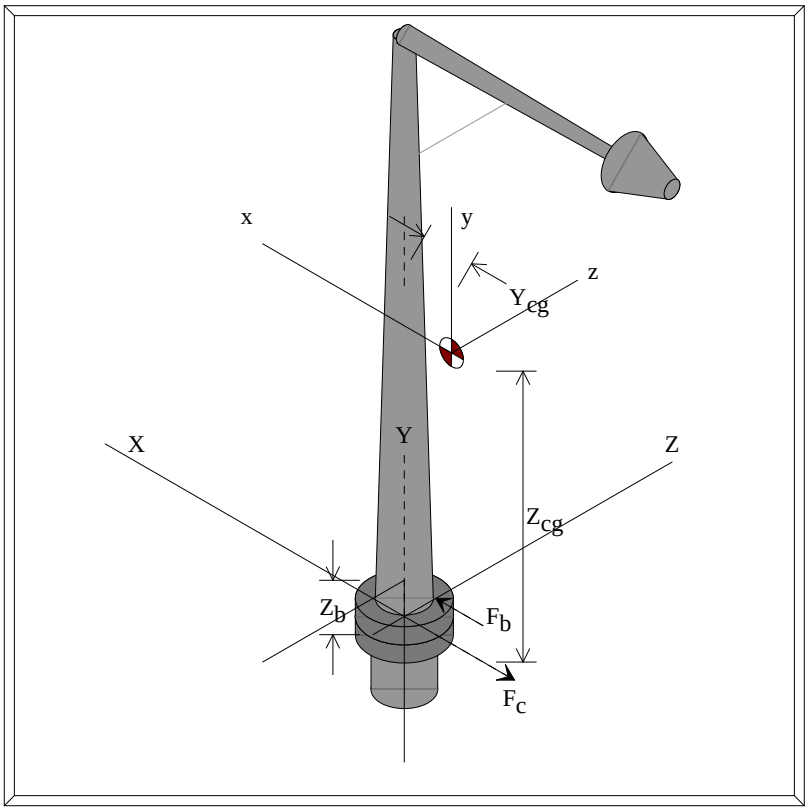

Figure 4.0.9

After this 100 milli-seconds, gravity acting on the currently free moving pole, the bottom plate of the coupler will contact the ground, and the pole will hopefully rotate **forward** along the path of the vehicle rather than falling back on top of the vehicle. This would be the preferred kinematics of the pole from a crashwothiness and damage/injury point of view.

This conclusion would be valid if there is little or no rotational kinetic energy in the pole at this point in time. Notice in **Figure 4.0.9** that the distance between the impact point and the shear coupler location is small, (approximately 6-10 inches) in comparison to the assumed vertical CG location of **255** inches above the coupler. This would suggest a small $\mathbf{M_X}$ moment about the pole's **x** inertial axis pass through the pole CG, and thus a small angular acceleration of the pole about the **x** axis. This would support the above conclusions of the perferred pole kinematics, but it is not conclusive proof.

This one-dimensional analysis has proven to be beneficial. It suggest that the characteristics of the pole kinematics after impact require further two-dimensional analysis.

The two dimensional analysis is presented in the next section **4.1**.

4.1 Dynamic Analysis (Two-Dimensional)

A typical highway lamp pole, for example the one shown in Figure 1.1, fitted with a break-away shear coupler is shown in **Figure 4.1.1**.

A coordinate system **X-Y-Z** is fixed at the center of the bottom plate of the shear coupler as shown in **Figure 4.1.1**. The bottom plate remains stationary as the shear coupler separates and as such the **X-Y-Z** coordinate system is fixed in space.

An additional inertial coordinate system **x-y-z** is attached to the **CG** of the light pole and placed initially parallel and perdendicular to the **fixed** coodinate system **X-Y-Z**.

The impacting vehicle motion is in the X direction and remains in the X-Y plane. The contact point of the vehicle bumper is at point **B** applying a force $\mathbf{F_b}$ to the pole. The shear coupler reacts with a force shown as $\mathbf{F_c}$ in **Figure 4.0.1**.

The load deflection characteristics of the vehicle bumper **Figure 4.0.6**, and that of the shear coupler, **Figure 4.0.3** for this two-dimensional analysis are the same as previously used in the one-dimensional analysis.

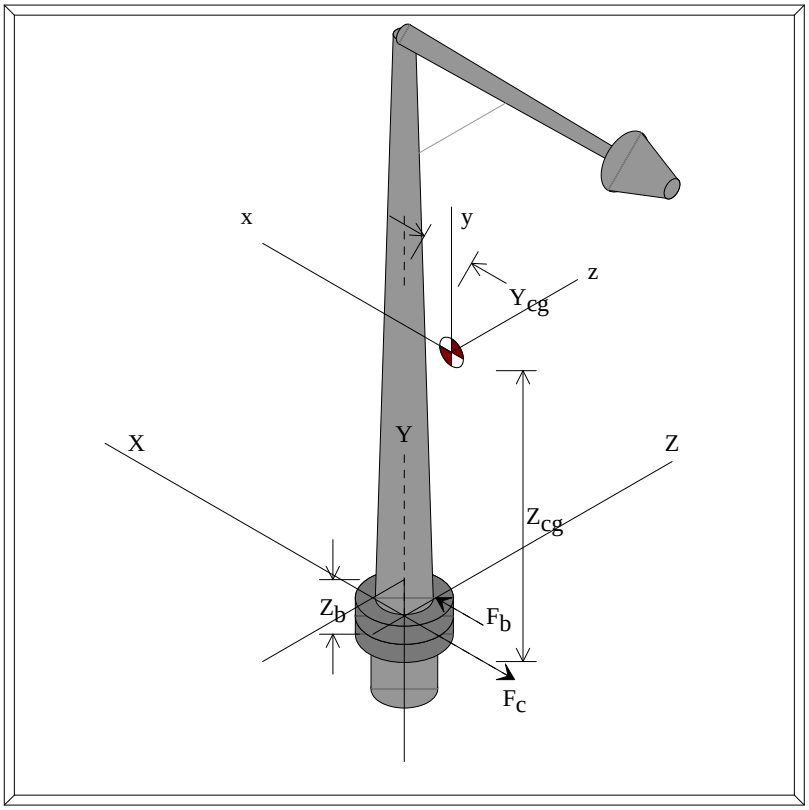

Figure 4.1.1

Equations of Motion for the impacting vehicle

The impacting vehicle is assumed a single point mass moving in and remaining in a plane $\mathbf{Z_b}$ distance above the light pole shear coupler, and $\mathbf{Z_b} + \mathbf{Z_c}$ vertical distance above the ground.

The vehicle is a single mass requiring only a single equation of motion.

$$F_{xv} = m_v * \ddot{x}_v \quad \text{---------- Eq. 4.1.1}$$

The pole requires three equations...

$$F_x = m * \ddot{x}$$

$$F_y = m * \ddot{y}$$

$$M_z = I_{zz} * \ddot{\theta}_z \quad \text{---------- Eq. 4.1.2}$$

Equation **4.1.1** and Equation Set **4.1.2**, represent a set of **4** simultaneous second order equations which are expanded to a set of **8** first order equations in Equation Set **4.1.3**.

The Equation Set is then solved numerically with a fourth order Runga-Kutta method. The expanded equation set is...

$$\dot{x}_v = q_1$$

$$\ddot{x}_v = \dot{q}_1 = \frac{1}{m_v} * \left[F_x\right]$$

$$\ddot{x} = q_2$$

$$\ddot{x} = \dot{q}_2 = \frac{1}{m} * \left[F_x\right]$$

$$\ddot{y} = q_3$$

$$\ddot{y} = \dot{q}_3 = \frac{1}{m} * \left[F_y\right]$$

$$\dot{\theta}_z = q_4$$

$$\ddot{\theta}_z = \dot{q}_4 = \frac{1}{I_{zz}} * \left[M_z\right] \qquad \text{Eq. 4.1.3}$$

This two-dimensional analysis provided resulting vehicle and pole motion in the X direction (horizontal) which as expected were the same the one-dimensional analysis.

Figure 4.1.2, the vehicle horizontal velocity time history provided by the two-dimensional model compared exactly with **Figure 4.0.7** provided by the one-dimensional analysis.

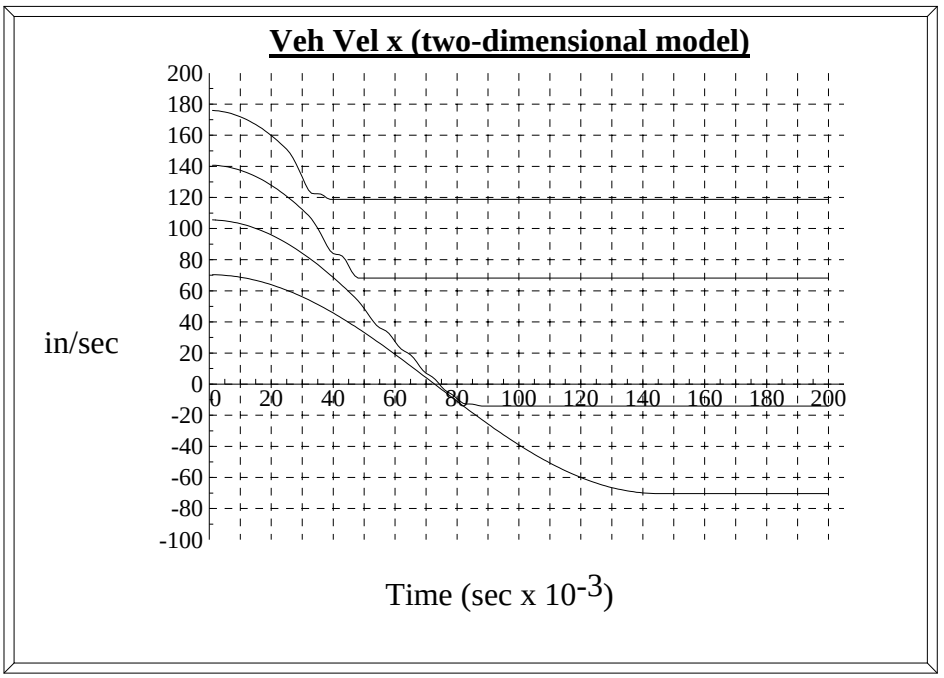

Figure 4.1.2

Figure 4.1.3, the pole horizontal velocity time history provided by the two-dimensional model compared exactly with **Figure 4.0.8** provided by the one-dimensional analysis.

The two-dimensional model however provides the vertical motion of the pole and the rotational motion of the pole about the **z** axis.

After about 3.5 inches of horizontal motion, the pole is clear of the bottom plate of the coupler and gravity contrls the further vertical motion.

Rotation about the **Z** axis is quite small, ranging between **0 rad/sec** angular velocity for impact velocities in excess of **12** mph to a computed maximum of **0.48 rad/sec** at **9-10** mph.

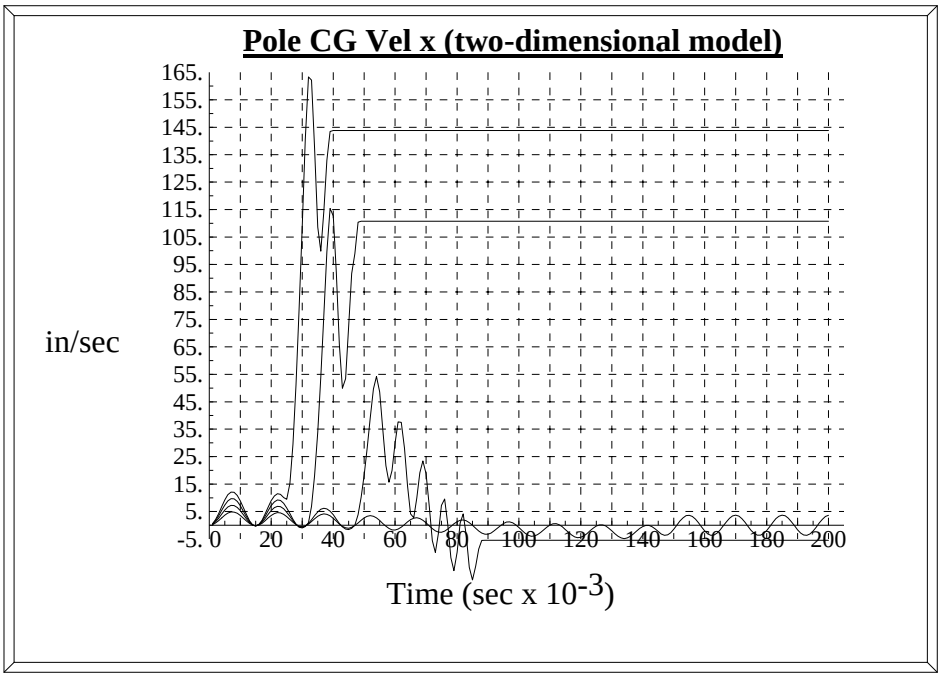

Figure 4.1.3

The discussion in **Section 4.0** regarding the horizontal velocity of the pole after impact being greater than the vehicle's reduced velocity continues to be verified by this two-dimensional analysis.

The pole's positive relative velocity with respect tot the vehicle, and the rotational angular velocity as a function of impact velocity in Mph is shown in **Figure 4.1.4** and **Figure 4.1.5**.

Results are indeed sensitive to the percent damping used in the numerical analysis, which ranged from 5% to 10% of critical, and the impact speed of the vehicle. Below and above 11 Mph having different trends. Even though the results are not as consistent as one would like, the important feature remains evident.

> After shear coupler failure, the pole leads the vehicle with a significant positive relative velocity (20-90 in/sec), and has little backward rotational velocity (0 to 0.5 rad/sec).

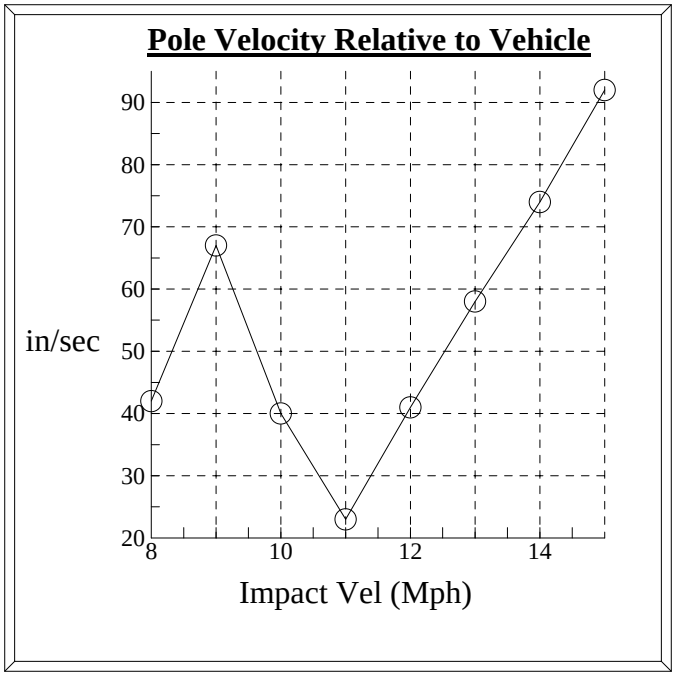

Figure 4.1.4

The energy due to this lateral horizontal velocity, $1/2M_pV^2$, is transformed into rotational energy, $1/2I_g\omega^2$, once the base of the pole contacts the ground. (I_g is the mass mment of inertia of the pole about the base contact point of rotation.)

$$\left(\frac{1}{2}\right) * M_p * \left(\dot{x}_p\right)^2 = \left(\frac{1}{2}\right) * I_g * \left(\dot{\theta}_z\right)^2$$

$$\dot{\theta}_z = \sqrt{\left(\frac{M_p}{I_g}\right) * \dot{x}_p^{\,2}} \qquad \text{Eq. 4.1.4}$$

The angular velocity of the pole immdeiately before the base contacts the ground is shown in (Black, bottom curve) in **Figure 4.1.5**. This rotation is postive, i.e. tending to rotate back on top of the impacting vehicle.

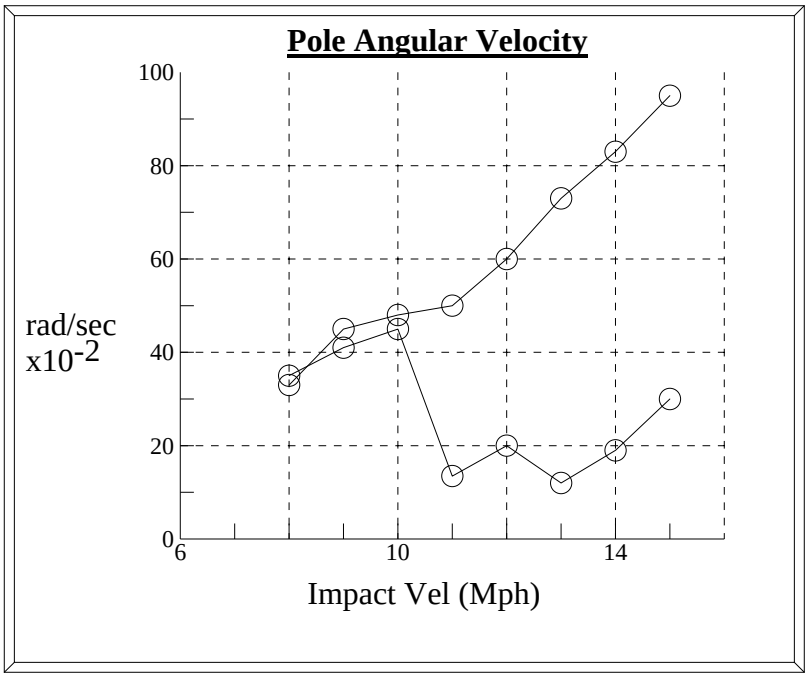

Figure 4.1.5

Equation **4.1.4** provides the available energy for negative rotational velocity, (red, top curve), **Figure 4.1.5**. This rotational velocity rotates the pole forward, away from the impacting vehicle.

These results suggest the following conclusions:

After shear coupler failure, the pole leads the vehicle with a significant positive relative velocity (20-90 in/sec), and has little backward rotational velocity (0 to 0.5 rad/sec).
As`the base of the pole contacts the ground, the rotation of the pole will reverse and rotate forward away from the path of the following vehicle.

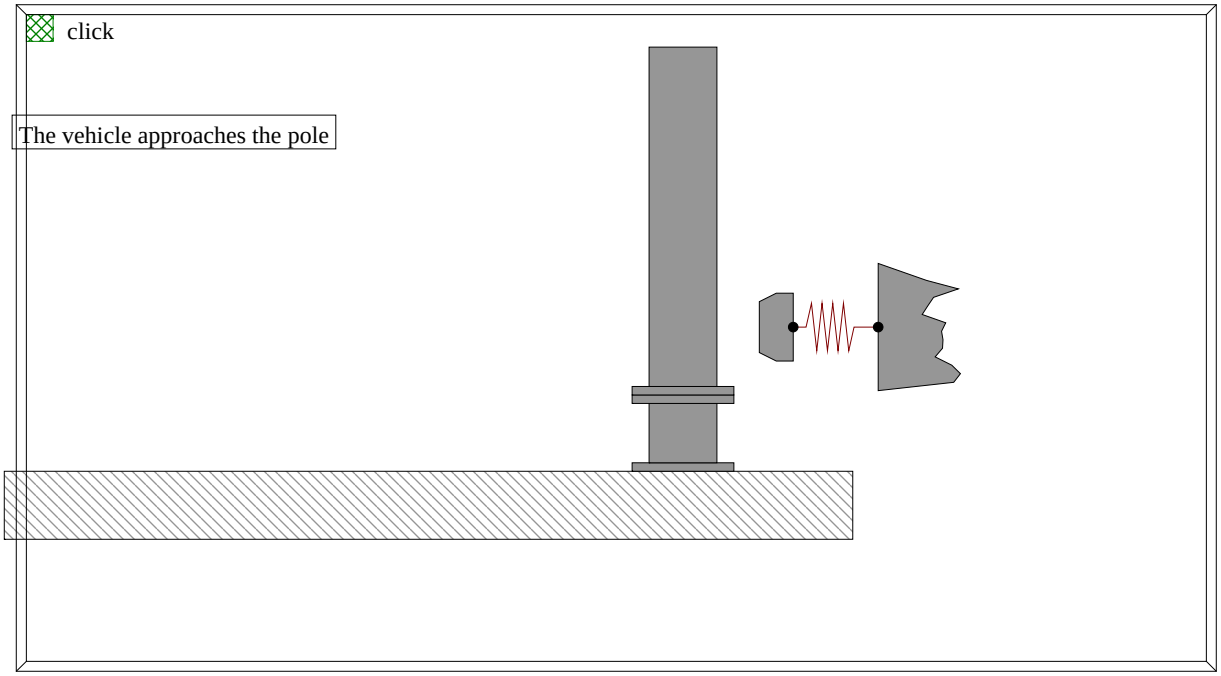

Figure 4.1.6

5.0 Conclusions and Recommendations

The results of the analysis qualify as **proof of concept**.

The analysis has focused on a generic steel highway light pole, shown in Figure 5.0.1, and utilizes a comparative analysis approach which may be extended to other pole sizes, as well as wooden telephone poles.

Adapting the **Shear Coupling** to wooden telephone poles presents fewer problems. Radial adjustable gusset plates, attached to both top and bottom plates, may be used to attach the **Shear Coupling** to the pole.

Such gussets may be incorporated within the current design without affecting the results of the analysis. Since telephone poles are subject to less torsion, this area of concern is reduced. Additionally, there are probably less restrictive code requirements.

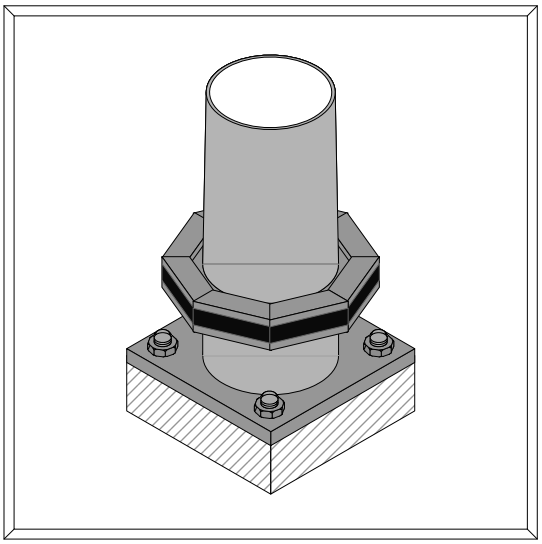

Figure 5.0.1

Advantages of the Shear Coupling

Clearly the most important aspect of the **Shear Coupling** is improved cost effective **crashworthness**.

Applicable to **new pole installations** as well as a **retrofit** for current poles at high risk or which have been damaged.

Utilizing the **Coupling** for vulnerable poles, thus eliminating the need of protective guard rails, may prove cost effective.

The **Shear Coupling** is **Omni-directional**.

All components are either easy to manufacture or are easy modifications of existing materials.

The **Shear Coupling** consists of reusable components. Reinstalling a damaged pole requires no expensive parts from the manufacturer, saving both time and money.

Once installed, de-masting and re-setting may prove cost effective for inspecting or maintaining poles.

In the event of a vehicle collision, the damage to the pole and specifically the base, is reduced or eliminated.

The reduced repair cost, reduced damage to the impacting vehicle, and reduced injury, could have a significant influence upon insurance liability and litigation considerations.